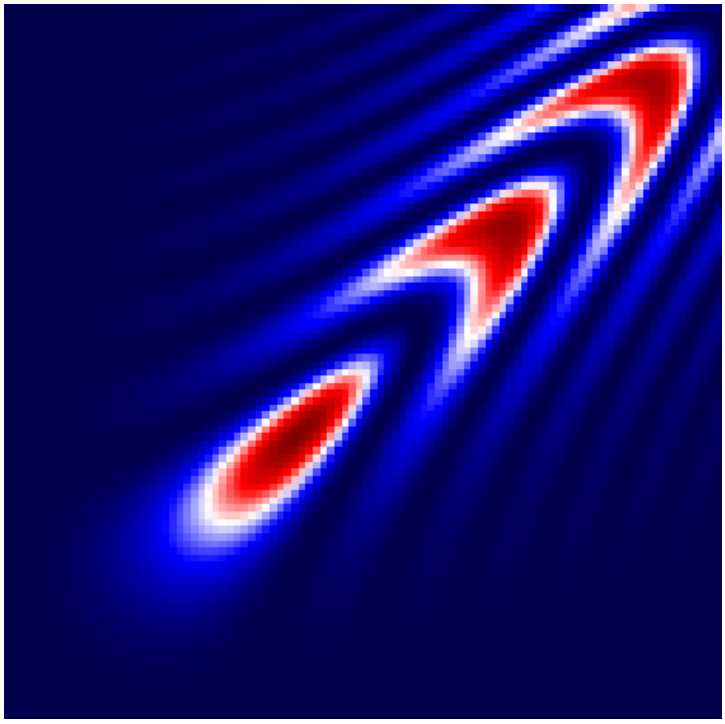

Analysis of selective photon addition in a bosonic mode with an ancillary qubit

Master's thesis in Complex Adaptive Systems

MARTIN JIRLOW

DEPARTMENT OF MICROTECHNOLOGY AND NANOSCIENCE

CHALMERS UNIVERSITY OF TECHNOLOGY
Gothenburg, Sweden 2024
www.chalmers.se

Master's thesis 2024

Analysis of selective photon addition in a bosonic mode by an ancillary qubit

MARTIN JIRLOW

CHALMERS
UNIVERSITY OF TECHNOLOGY

Department of Microtechnology and Nanoscience
Division of Applied Quantum Physics
Chalmers University of Technology
Gothenburg, Sweden 2024

Analysis of selective photon addition in a bosonic mode by an ancillary qubit
MARTIN JIRLOW

Supervisor: Tahereh Abad, Department of Microtechnology and Nanoscience
Examiner: Göran Johansson, Department of Microtechnology and Nanoscience

Master's Thesis 2024
Department of Microtechnology and Nanoscience
Division of Applied Quantum Physics
Chalmers University of Technology
SE-412 96 Gothenburg
Telephone +46 31 772 1000

Cover: Chevron pattern simulated using QuTiP for the $|0g\rangle \rightarrow |1e\rangle$ transition using the SNAPPA gate.

Typeset in LaTeX
Gothenburg, Sweden 2024

Analysis of selective photon addition in a bosonic mode by an ancillary qubit
MARTIN JIRLOW
Department of Microtechnology and Nanoscience
Chalmers University of Technology

Abstract

Quantum computation using bosonic modes is a promising alternative to discrete quantum computing with superconducting qubits. Bosonic modes utilize microwave cavities to encode and manipulate quantum information, leveraging the equally spaced energy levels of the cavity to create multi-photon states for robust encoding of quantum information. The dominant source of error in a bosonic mode is single-photon loss, and finding error correction protocols for this error is an active area of research.
Autonomous quantum error correction for a bosonic code was first applied experimentally by Gertler et. al. [J. M. Gertler et al., Nature 590, 243 (2021)], yet they did not reach the break-even point. An alternative protocol for recovering the cavity state after a photon loss is to apply a Selective Number-dependent Arbitrary-Phase Photon-Addition (SNAPPA) gate [M. Kudra et al., arXiv: 2212.12079 (2021)] followed by a quick qubit reset. SNAPPA was implemented experimentally by Kudra et al. yet no accurate theoretical model for this process exists.
We derive an accurate and effective Hamiltonian for the SNAPPA gate, and simulate the dynamics to find close agreement with previous experimental results. The derivation highlights a general procedure for finding effective Hamiltonians where current procedures previously have failed.

Acknowledgements

I would like to express my heartfelt gratitude to my supervisor, Tahereh Abad, for giving me the opportunity to work on this project and for her ever present guidance and support. I would also like to thank Axel Eriksson and Simone Gasparinetti for many fruitful discussions and invaluable feedback throughout this project. I would also like to extend my gratitude to my examiner, Göran Johansson. I am also grateful to my opponent, Alex Maltesson, for our insightful discussions and his useful feedback.
Last but not least, the deepest appreciation for my family and friends for their undying support.

Martin Jirlow, Gothenburg, June 2024

Contents

List of Figures

List of Tables

1
Introduction

A quantum computer uses principles of quantum mechanics to solve computational problems that are difficult for classical computers. The concept of a quantum computer was first introduced by Feynman [1] in 1982. Since then, the potential applications of quantum computers have been theorized in a multitude of fields. In 1994, Shor [2] showed how a universal quantum computer could be leveraged for an efficient algorithm for the prime factoring of large numbers, a problem intractable for classical computers. It also has potential application in quantum chemistry [3] and for solving the travelling salesman problem [4], and more.

The computational unit of a quantum computer is the qubit, a two-level quantum system and the quantum equivalent to a classical bit. There are many physical platforms for realizing qubits, including electron spins, quantum dots, trapped ions, and polarized photons [5]. In this thesis we focus on the platform of superconducting circuits; by utilizing a superconducting Josephson junction, one can engineer an anharmonic oscillator circuit which can be used as a quantum two-level system, and thus leveraged as a qubit. This is referred to as a superconducting transmon qubit [5].

A transmon qubit, like all qubit architectures, is sensitive to errors. These errors must be protected against lest they accumulate and yield inaccurate results during a computation. The field of quantum error correction (QEC) seeks to develop frameworks for this purpose. A conventional approach to QEC for transmon qubits is to construct logical qubits out of many physical qubits in order to increase robustness [6], for example using surface codes [7]. This increases the engineering complexity of the system and introduces more error sources, as each added hardware component can lead to unwanted cross-talk between components [6]. An alternative approach is to encode the logical qubit information in the bosonic modes of a harmonic oscillator, often referred to as continuous variable (CV) quantum computing.

1.1 Continuous variable quantum computing

In superconducting quantum electrodynamics, CV systems are realized by coupling a superconducting microwave cavity to a non-linear element, for example a transmon qubit [6]. The non-linearity is necessary for universal control of the cavity state, through dispersive interactions between the qubit and cavity [8, 9]. The equally spaced energy levels of the cavity are used to encode the qubit information in ways that allow for hardware-efficient quantum error correction. The schemes used for encoding the quantum information in the cavity are known as bosonic codes [6].

The dominant source of error in a bosonic mode is single-photon loss [6, 10, 11]. Several bosonic codes have been developed to be robust against this, including the binomial codes [12] and cat codes [10, 11]. The codewords for these codes consist of superpositions of Fock states with equal parity; states with only odd or only even photon numbers. In the event of a single-photon loss, the Fock states and consequently the codewords change parity. Repeated measurement of the state parity can then detect single-photon loss events, and the error can be corrected for with a unitary operator that maps the error states back to the logical codewords [13, 14]. Ofek et al. [13] demonstrated how this QEC approach can reach the break-even point, where the lifetime of the corrected logical qubit extends the lifetime of the cavity itself. These QEC approaches have the drawback that they require constant measurement of the parity error syndrome. This measurement must not itself interfere with the cavity state (which is known as a quantum non-demolition (QND) measurement), however the measurement itself is not fault-tolerant and can introduce unwanted errors for the QEC protocol [13, 15, 16].

A way to avoid the problem of error syndrome measurement is to design error correction protocols that do not require QND measurements of the cavity state. These are known as autonomous quantum error correction (AQEC) protocols. They instead rely on unitary operations which selectively only targets error states in the cavity, while leaving the logical codes of the bosonic code intact [16–18]. Gertler et al. [17] realized Parity Recovery by Selective Photon Addition (PReSPA) for the selective addition of photons to only even-parity Fock states in the cavity state, effectively correcting single-photon losses in bosonic encodings with parity codewords.

1.2 Selective number-dependent arbitrary-phase photon-addition

PReSPA has the disadvantage that it requires a complicated drive protocol to realize the operation, which is driven continuously. This limits the application of PReSPA; if one desired to perform AQEC using a pulsed version of PReSPA the pulses would have to be long to not drive unwanted transitions [18]. Kudra et al. [18] introduced and experimentally realized an alternative to PReSPA, by applying a Selective Number-dependent Arbitrary-Phase Photon-Addition (SNAPPA) gate. SNAPPA operates with a simpler driving scheme yet is able to perform selective photon addition similar to PReSPA. However, the derived effective Hamiltonian did not agree with the experimental results, requiring theoretically unfounded fitting parameters as well as a cross-talk term added to the cavity and qubit stark shifts in order to match the experimental data. The same derivation used in Kudra et al. [18] is also used in Campagne-Ibarcq et al. [19], where the theoretical model also does not fit with experimental data.

In this thesis, we show that the originally derived model is not a proper description of the physical system. We derive an effective Hamiltonian for the SNAPPA gate that agrees with the experimental data from Kudra et al. [18], demonstrated with the aid of numerical simulation. We also identify the errors in the original derivation which highlights the general problem with the derivation approach used.

This thesis is structured as follows: in Chapter 2 we introduce the necessary theoretical background and present the SNAPPA gate in more detail. In Chapter 3 we derive the effective Hamiltonian for the SNAPPA gate, and in Chapter 4 we present the results of simulating the derived Hamiltonian, and compare it to experimental data. In Chapter 5 we conclude by summarizing and discussing our results.

2

Theory

In this chapter we summarize the necessary theoretical background for this thesis. We will assume some familiarity with quantum mechanics and linear algebra.

Recall that a pure state of a quantum system is a non-zero element in a complex Hilbert space $\mathcal{H}$. The time evolution of a quantum state $|\psi\rangle$ is governed by the Schrödinger equation

$$i\hbar\frac{\partial}{\partial t}|\psi\rangle = \hat{H}(t)|\psi\rangle\,, \tag{2.1}$$

where $\hbar$ is the reduced Planck's constant, and $\hat{H}(t)$ is the Hamiltonian of the system. In this thesis, we work in a system of units such that $\hbar = 1$. The Schrödinger equation shows that in order to understand a quantum system, we need to have an accurate description of its Hamiltonian, $\hat{H}(t)$. Modeling a quantum system is the challenge of finding this Hamiltonian.

This chapter is structured as follows: we begin by introducing the components for our system, and their Hamiltonians, in Section 2.1. We then describe how these can be utilized for what is known as continuous variable quantum computing in Section 2.2. In Section 2.3 we describe the SNAPPA gate, the main focus of this thesis. Finally, in Section 2.4 we describe the analytical tools we use for modelling the SNAPPA gate.

2.1 Circuit quantum electrodynamics

We begin by first introducing the hardware elements used for constructing superconducting quantum computers, in an architecture known as circuit quantum electrodynamics. These components utilize superconducting phenomena in order to create highly non-classical, controllable quantum systems which can be utilized to store and manipulate quantum information.

2.1.1 The superconducting transmon qubit

The computational unit of a quantum computer is the qubit. A qubit is a quantum system whose Hilbert space contains a subspace isomorphic to $\mathbb{C}^2$, the two dimensional vector space over the field of complex numbers. We often use the com-

putational basis for this subspace, spanned by the basis vectors [20]

$$|0\rangle = \begin{bmatrix} 1 \\ 0 \end{bmatrix}, \tag{2.2}$$

$$|1\rangle = \begin{bmatrix} 0 \\ 1 \end{bmatrix}. \tag{2.3}$$

A general qubit state $|\psi\rangle$ can be written as

$$|\psi\rangle = c_0 |0\rangle + c_1 |1\rangle, \tag{2.4}$$

where c_0 and c_1 are complex coefficients. The Born rule also requires that our state is normalized, which gives

$$|\langle\psi|\psi\rangle|^2 = |c_0|^2 + |c_1|^2 = 1. \tag{2.5}$$

Writing c_1 and c_2 in polar form, $c_0 = r_0 e^{i\eta}$, $c_1 = r_1 e^{i\varphi}$, we get

$$|\psi\rangle = r_0 e^{i\eta} |0\rangle + r_1 e^{i\varphi} |1\rangle = e^{i\eta} \left(r_0 |0\rangle + r_1 e^{i(\varphi-\eta)} |1\rangle \right). \tag{2.6}$$

Here η is a global phase, which has no physical significance for a quantum state. Combining this with (2.5) we can write (2.4) as

$$|\psi\rangle = \cos\frac{\theta}{2} |0\rangle + e^{i\phi} \sin\frac{\theta}{2} |1\rangle, \tag{2.7}$$

where $\theta \in [0, \pi]$ and $\varphi - \eta = \phi \in [0, 2\pi)$ are spherical angles, which are sufficient to fully describe a qubit state. [20, 21]

There are many ways to physically construct a qubit [5, 22–24]. One approach is to utilize the anharmonic energy spectrum of a superconducting circuit (see Figure 2.1) consisting of a capacitor with energy E_C connected in parallel to a Josephson junction; a nonlinear, superconducting circuit element with Josephson energy E_J. Energy will oscillate in this system, alternating between the capacitor and junction. This allows us to store quantum information in the energy levels of the oscillator. It is common to engineer the circuit such that $E_J \gg E_C$, and a qubit in this regime is called a transmon qubit. Such a circuit can be quantized to arrive at the Hamiltonian [5, 25]

$$\hat{H}_{\text{transmon}} = \omega_q \hat{b}^\dagger \hat{b} - \frac{E_J}{4!} \left[\varphi_q (\hat{b} + \hat{b}^\dagger) \right]^4, \tag{2.8}$$

where $\hat{b}$ ($\hat{b}^\dagger$) is the annihilation (creation) operator of the qubit. Eigenstates of the Hamiltonian are referred to as Fock states, or number states, and are labeled $|n\rangle$ where $n \geq 0$. $|0\rangle$ is the lowest energy eigenstate of the system, often called the ground state or vacuum state. The annihilation and creation operators annihilate or create an excitation in the qubit, respectively. Their action on Fock states is described by

$$\hat{b} |n\rangle = \sqrt{n} |n-1\rangle, \tag{2.9}$$

$$\hat{b}^\dagger |n\rangle = \sqrt{n+1} |n+1\rangle. \tag{2.10}$$

They allow us to climb the energy ladder of the oscillator, and are therefore referred to as ladder operators.

The fourth order term in (2.8) can be expanded, and fast rotating terms can be ignored (see Section 2.4.3), to obtain the Hamiltonian

$$\hat{H}_{\text{transmon}} = \omega_q \hat{b}^\dagger \hat{b} - \frac{\alpha}{2} \hat{b}^\dagger \hat{b}^\dagger \hat{b} \hat{b}, \tag{2.11}$$

where α is the anharmonicity of the qubit.

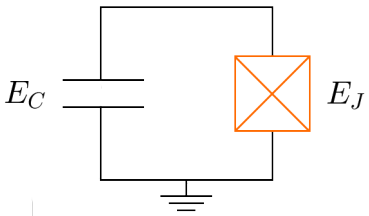

Figure 2.1: Circuit diagram of a superconducting qubit, consisting of a capacitor (left) with energy E_C and a Josephson junction (in orange) with Josephson energy E_J.

The energy of a Fock state $|n\rangle$ of the anharmonic oscillator is

$$\langle n|\hat{H}_{\text{transmon}}|n\rangle = \omega_q n - \frac{\alpha}{2} n(n-1). \tag{2.12}$$

The energy difference between two subsequent Fock states is therefore

$$\langle n+1|\hat{H}_{\text{transmon}}|n+1\rangle - \langle n|\hat{H}_{\text{transmon}}|n\rangle = \omega_q - \alpha n, \tag{2.13}$$

which tells us that the transition energy between $|0\rangle$ and $|1\rangle$ is different from that between higher energy states. This means that we can selectively drive the $|0\rangle - |1\rangle$ transition without transitioning to higher energy levels, assuming the anharmonicity is large enough. We can therefore selectively address the subspace spanned by $\{|0\rangle, |1\rangle\}$, effectively functioning as a qubit. In this thesis, we sometimes refer to the basis states $\{|0\rangle, |1\rangle\}$ of a qubit as $\{|g\rangle, |e\rangle\}$, the *ground* and *excited* states, to avoid confusion with the number states of a harmonic oscillator, introduced in 2.1.2.

2.1.2 Microwave cavity and coupling

A 3D cavity is a type of electromagnetic resonator. It consists of a largely closed metallic structure, which is either hollow or filled with a dielectric material. The cavity can then confine photons that match the resonance frequency of the cavity. When this resonance frequency is in the microwave (radio frequency) regime, it is often called a microwave cavity. A superconducting microwave cavity can be modelled as a harmonic oscillator, with the Hamiltonian [5]

$$\hat{H}_{\text{cavity}} = \omega_a \hat{a}^\dagger \hat{a}, \tag{2.14}$$

where $\hat{a}$ ($\hat{a}^\dagger$) is the annihilation (creation) operator for the cavity mode and ω_a is the frequency of the cavity. It follows that the harmonic oscillator has equally

spaced energy levels, unlike the anharmonic oscillator, and the Hilbert space of the harmonic oscillator is infinite.

A cavity can be coupled to a superconducting qubit, allowing them to interact with each other. The Hamiltonian of this system can be described by

$$\hat{H} = \hat{H}_{\text{cavity}} + \hat{H}_{\text{transmon}} + \hat{H}_{\text{int}}, \tag{2.15}$$

where the interaction term $\hat{H}_{\text{int}}$ is given by [5]

$$\hat{H}_{\text{int}} = -g(\hat{b} - \hat{b}^\dagger)(\hat{a} - \hat{a}^\dagger), \tag{2.16}$$

where g is the coupling strength. Inserting (2.8), (2.14) and (2.16) in (2.15) gives

$$\hat{H} = \omega_a \hat{a}^\dagger \hat{a} + \omega_q \hat{b}^\dagger \hat{b} - \frac{E_J}{4!}\left[\varphi_q(\hat{b} + \hat{b}^\dagger)\right]^4 - g(\hat{b} - \hat{b}^\dagger)(\hat{a} - \hat{a}^\dagger). \tag{2.17}$$

When coupling two quantum systems in general, the coupled system Hilbert space is the tensor product of the component spaces,

$$\mathcal{H}_{\text{system}} = \mathcal{H}_{\text{cavity}} \otimes \mathcal{H}_{\text{qubit}}, \tag{2.18}$$

and the basis states in this Hilbert space are tensor products between basis states of the component systems. For example, using the Fock basis

$$\text{span}\{|n\rangle_{\text{cavity}} \otimes |m\rangle_{\text{qubit}} : n \geq 0, m \geq 0\} = \mathcal{H}_{\text{system}}. \tag{2.19}$$

The product $|n\rangle_{\text{cavity}} \otimes |m\rangle_{\text{qubit}}$ is often written $|n\rangle\,|m\rangle$ or simply $|nm\rangle$.

The interaction between the qubit and cavity is heavily dependent on the difference between the qubit and cavity frequencies, $|\omega_a - \omega_q|$, and the coupling strength g. If $g/|\omega_a - \omega_q| \gtrsim 1$, the interaction is strong, and likely to cause photons to be exchanged between the qubit and cavity. If instead $g/|\omega_a - \omega_q| \ll 1$, then no excitation exchange occurs, however the interaction still affects the energy spectrums of the two components. This is known as the dispersive regime. In the dispersive regime, (2.17) can be written in the normal mode basis as [26]

$$\hat{H} = \tilde{\omega}_a \hat{a}^\dagger \hat{a} + \tilde{\omega}_q \hat{b}^\dagger \hat{b} - \frac{E_J}{4!}\phi^4, \tag{2.20}$$

where $\phi = \varphi_q(\hat{b} + \hat{b}^\dagger) + \varphi_a(\hat{a} + \hat{a}^\dagger)$, and $\tilde{\omega}_a$ and $\tilde{\omega}_q$ are the normal mode frequencies of the cavity and qubit, which are generally different from the bare mode frequencies in (2.17). However, in the dispersive regime, $\tilde{\omega}_a, \tilde{\omega}_q \approx \omega_a, \omega_q$ [26]. The coefficients φ_q and φ_a are referred to as the participation ratios of the qubit and cavity respectively. This Hamiltonian is often approximated (using the rotating wave approximation, which we introduce in Section 2.4.3) to [25]

$$\hat{H} = \omega_a \hat{a}^\dagger \hat{a} - \frac{K_c}{2}\hat{a}^\dagger \hat{a}^\dagger \hat{a}\hat{a} + \omega_q \hat{b}^\dagger \hat{b} - \frac{\alpha}{2}\hat{b}^\dagger \hat{b}^\dagger \hat{b}\hat{b} - \chi \hat{b}^\dagger \hat{b}\hat{a}^\dagger \hat{a}, \tag{2.21}$$

where K_c is the cavity Kerr non-linearity, and χ is the dispersive shift. The Kerr non-linearity is a small anharmonicity due to the coupling between the cavity and qubit modes. Usually, K_c is of the order of kHz, while α is on the order of a few

hundred MHz. Since the Kerr non-linearity is of a much smaller scale than the other energy scales of the system, the cavity can still be utilized as a harmonic oscillator but with a small error induced by K_c. The dispersive shift χ is a shift of the energy of the system dependent on the number of photons in both qubit and cavity. The dispersive shift is crucial for selective control of the cavity Fock states, as we will see in Section 2.3. Microwave cavities are of great importance for continuous variable quantum computing, discussed in Section 2.2.

2.1.3 Controlling qubit and cavity states

We can control a superconducting qubit or cavity by coupling the components to microwave sources, often referred to as drives [5]. The Hamiltonian corresponding to a sinusoidal microwave drive on the qubit can be written as

$$\hat{H}_d = \frac{\varepsilon}{2}\left(\hat{b}e^{i\omega_d t} + \hat{b}^\dagger e^{-i\omega_d t}\right), \tag{2.22}$$

where ε is the drive amplitude, and ω_d is the drive frequency.

If the drive frequency is the same as the qubit or cavity frequency, the drive is said to be resonant with the qubit or cavity. This promotes high excitation exchange between the driving microwave field and the component, and can be effectively used to change the excitation of a component.

If the drive frequency is slightly detuned from the qubit frequency by some detuning Δ such that $\omega_d = \omega_q + \Delta$, the probability of excitation exchange greatly decreases as $|\Delta|$ increases. However, off-resonant drives can shift the resonance frequencies of the system, which is known as a Stark shift [5, 25].

2.2 Continuous variable quantum computing

In Section 2.1 we discussed how a two-level system known as a qubit can be used to store quantum information. However, this is not the only way to utilize superconducting circuits for quantum computation. An alternative to storing the information in the qubit is to instead store it in the cavity, allowing for a different approach to error correction and control [27–29]. This is accomplished with bosonic codes.

2.2.1 Bosonic codes

A microwave cavity is modelled as a harmonic oscillator, with equally spaced energy levels. We can therefore not address the two lowest energy levels as a qubit like we can with the anharmonic oscillator; driving the $|0\rangle - |1\rangle$ transition would also drive transitions to higher energy levels. Instead we need to encode the qubit state in the cavity, using what is known as a bosonic code. A cavity used for this purpose is known as a bosonic qubit. When a cavity coupled to a qubit is utilized in this way, the qubit is often referred to as an ancillary qubit, or ancilla, since it does not store the computational state of the system. [6]

A bosonic code is a method of encoding a logical qubit state

$$|\psi_L\rangle = c_0 |0_L\rangle + c_1 |1_L\rangle, \tag{2.23}$$

in the equally spaced energy levels of a microwave cavity. We do this by mapping the logical qubit states $\{|0_L\rangle, |1_L\rangle\}$ to a bosonic state in the cavity. Choosing the encoding properly is crucial for efficient error mitigation and effective control of the cavity state. [6]

The dominant error source in a microwave cavity is single photon loss from interaction with the environment [11], described by the action of the annihilation operator $\hat{a}$. Many bosonic codes are designed to be robust against such losses, for example the four-component cat code [11]. These codes often require procedures for restoring photons in the cavity when a single-photon loss event occurs. It is therefore of interest to find error correction protocols for single photon losses [6]. One such protocol is the proposed Selective Number-dependent Arbitrary-Phase Photon-Addition (SNAPPA) gate [18], which we describe in more detail in Section 2.3.

2.3 The SNAPPA gate

Kudra et al. [18] introduced a gate to add photons selectively to cavity Fock states. This gate is called a Selective Number-dependent Arbitrary-Phase Photon-Addition (SNAPPA) gate, and can be described by [18]

$$S_{\mathrm{PA}}(\{(\theta_i)_{n_i \to n_{i+1}}\}) = \sum_{i \subset N} e^{i\theta_i} |n_{i+1}\rangle |e\rangle \langle n_i| \langle g| + h.c., \tag{2.24}$$

where $|n_i\rangle$ are the cavity Fock states selectively targeted by the gate, and θ_i is an arbitrary phase-shift that we want the new states to acquire, and $\{|g\rangle, |e\rangle\}$ are the ground and first excited state of the ancillary qubit. When paired with a bosonic code that splits the Hilbert space into a code subspace and an error subspace with respect to photon-number parity, SNAPPA can be used to map the error subspace back to the code subspace, without affecting states in the code subspace [18]. This is illustrated in the energy level diagram in Figure 2.2. If SNAPPA is followed by a quick qubit reset to restore the qubit state; this could be used for autonomous error correction [18].

We see that the SNAPPA gate performs a two-photon transition $|n_i\rangle |g\rangle \to |n_i + 1\rangle |e\rangle$, by adding a photon excitation to both the cavity and the qubit simultaneously. This can then be followed by a quick, unconditional qubit reset to restore the state $|n_i + 1\rangle |g\rangle$.

To illustrate the SNAPPA gate, we focus on driving only a single selective transition for some n_i without a phase shift, $\theta_i = 0$. As a reminder, the Hamiltonian for the system, $\hat{H}_0$, is given by (2.21). The drive Hamiltonian when targeting only a single transition is

$$\hat{H}_d = \frac{\varepsilon_1}{2}\left(\hat{b}e^{i\omega_1 t} + \hat{b}^\dagger e^{-i\omega_1 t}\right) + \frac{\varepsilon_2}{2}\left(\hat{a}e^{i\omega_2 t} + \hat{a}^\dagger e^{-i\omega_2 t}\right), \tag{2.25}$$

where ε_1, ω_1 is the drive amplitude and frequency for the qubit drive, and ε_2, ω_2 is the drive amplitude and frequency for the cavity drive. The total Hamiltonian for

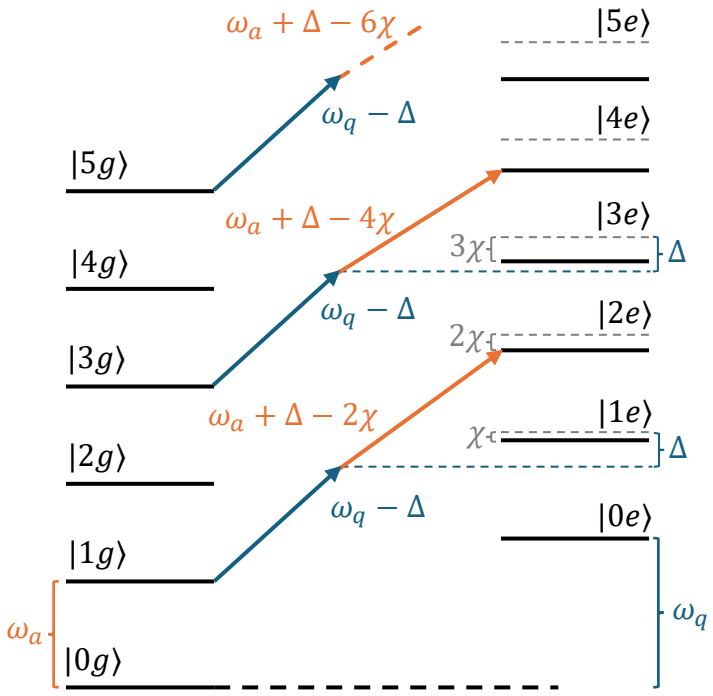

Figure 2.2: Level diagram of the SNAPPA gate mapping the odd parity subpace to the even parity subspace in the cavity.

this system is therefore

$$\begin{aligned}\hat{H}_{\text{PA}} = \omega_a \hat{a}^\dagger \hat{a} - \frac{K_c}{2}\hat{a}^\dagger\hat{a}^\dagger\hat{a}\hat{a} + \omega_q \hat{b}^\dagger\hat{b} - \frac{\alpha}{2}\hat{b}^\dagger\hat{b}^\dagger\hat{b}\hat{b} - \chi\hat{b}^\dagger\hat{b}\hat{a}^\dagger\hat{a} \\ + \frac{\varepsilon_1}{2}\left(\hat{b}e^{i\omega_1 t} + \hat{b}^\dagger e^{-i\omega_1 t}\right) + \frac{\varepsilon_2}{2}\left(\hat{a}e^{i\omega_2 t} + \hat{a}^\dagger e^{-i\omega_2 t}\right).\end{aligned} \tag{2.26}$$

The selectivity of the SNAPPA gate comes from the dispersive shift, χ. We are driving a two-photon transition, adding a photon to both qubit and cavity simultaneously. Since we are adding excitation to both qubit and cavity, the energy contribution from the dispersive term $\chi\hat{b}^\dagger\hat{b}\hat{a}^\dagger\hat{a}$ changes. This causes the transition frequency of the $|n_i\rangle|g\rangle \rightarrow |n_i+1\rangle|e\rangle$ transition to decrease depending on n_i; this frequency is given by [18]

$$\omega_{|n_i\rangle|g\rangle\rightarrow|n_i+1\rangle|e\rangle} = \omega_q + \omega_a - (n_i+1)\chi. \tag{2.27}$$

By choosing our drive frequencies such that $\omega_1 + \omega_2 = \omega_{|n_i\rangle|g\rangle\rightarrow|n_i+1\rangle|e\rangle}$ we can effectively drive this transition. We want to simultaneously avoid driving single-photon transitions in the qubit and cavity, as this introduces unwanted errors. We therefore choose our drives to be off-resonant with drive detuning Δ according to [18]

$$\omega_1 = \omega_q - \Delta, \tag{2.28}$$
$$\omega_2 = \omega_a + \Delta - (n_i+1)\chi. \tag{2.29}$$

In Kudra et al. [18] they derive an effective Hamiltonian for the SNAPPA gate of the form

$$\begin{aligned}\hat{H}(t) = \delta_{\text{Stark},q}\hat{b}^\dagger\hat{b} + \delta_{\text{Stark},a}\hat{a}^\dagger\hat{a} - \frac{\alpha}{2}\hat{b}^{\dagger 2}\hat{b}^2 - \frac{K_c}{2}\hat{a}^{\dagger 2}\hat{a} - \chi\hat{b}^\dagger\hat{b}\hat{a}^\dagger\hat{a} \\ + \left[g_{\text{eff}}e^{i(n_i+1)\chi t}\hat{b}^\dagger\hat{a}^\dagger + h.c.\right],\end{aligned} \tag{2.30}$$

where

$$\delta_{\text{Stark},q} = -2\alpha\eta_1\left(\frac{\varepsilon_1}{\Delta_1}\right)^2 - \chi\eta_2\left(\frac{\varepsilon_2}{\Delta_2}\right)^2 - \chi\eta_{12}\left(\frac{\varepsilon_1}{\Delta_1}\right)\left(\frac{\varepsilon_2}{\Delta_2}\right), \tag{2.31}$$

$$\delta_{\text{Stark},a} = -\chi\eta_1\left(\frac{\varepsilon_1}{\Delta_1}\right)^2 - 2K_c\eta_2\left(\frac{\varepsilon_2}{\Delta_2}\right)^2 - \chi\eta_{12}\left(\frac{\varepsilon_1}{\Delta_1}\right)\left(\frac{\varepsilon_2}{\Delta_2}\right), \tag{2.32}$$

$$g_{\text{eff}} = -\chi\eta_{\text{amp}}\sqrt{\eta_1\eta_2}\left(\frac{\varepsilon_1}{\Delta_1}\right)\left(\frac{\varepsilon_2}{\Delta_2}\right), \tag{2.33}$$

and $\Delta_1 = \omega_q - \omega_1$, $\Delta_2 = \omega_a - \omega_2$. However, the η parameters above are fitting parameters that do not arise naturally from the derivation. In order for (2.30) to match the experimental results, these parameters were fitted to [18]

$$(\eta_1, \eta_2, \eta_{12}, \eta_{\text{amp}}) = (0.09, 0.84, 4.68, 0.02)\,. \tag{2.34}$$

Since these parameters lack physical motivation, it is of interest to find a more accurate effective Hamiltonian analytically to match with the experimental data, which we do in Chapter 3.

2.4 Average Hamiltonian theory

When modelling quantum systems, it is often desireable to rewrite the original Hamiltonian into an effective Hamiltonian; an approximation of the system dynamics that is easier to grasp analytically, and can often be more efficiently simulated.

There are many methods and techniques for finding effective Hamiltonians, depending on the properties of the system. Unitary transformations are often used to change the reference frame of the system, possibly simplifying the Hamiltonian. One can also ignore terms that rotate rapidly compared to the time scale of the dynamics, using the rotating wave approximation.

2.4.1 Unitary transformations

An operator $\hat{U}(t)$ is unitary if $\hat{U}(t)^\dagger\hat{U}(t) = \hat{U}(t)\hat{U}(t)^\dagger = 1$ at all times t. A unitary operator preserves the inner products of vectors, and therefore also preserves orthonormality. It effectively transforms an orthonormal basis into another orthonormal basis, and can therefore be regarded as a change of basis. Furthermore, any unitary operator is related to some Hermitian operator $\hat{A}(t)$ through [20]

$$\hat{U}(t) = e^{\hat{A}(t)}. \tag{2.35}$$

A unitary operator can be used to transform a Hamiltonian according to the rule

$$\hat{H}'(t) = \hat{U}(t)\hat{H}(t)\hat{U}(t)^\dagger + i\frac{\partial \hat{U}}{\partial t}(t)\hat{U}(t)^\dagger. \tag{2.36}$$

Any product of operators $\hat{B}\hat{C}$ transformed by $\hat{U}\hat{B}\hat{C}\hat{U}^\dagger$ can be calculated as

$$\hat{U}\hat{B}\hat{C}\hat{U}^\dagger = \hat{U}\hat{B}\hat{U}^\dagger\hat{U}\hat{C}\hat{U}^\dagger. \tag{2.37}$$

It is therefore sufficient to transform the individual operators independently and inserting them in the original equation. This is useful since all the terms in the Hamiltonian considered in this thesis have terms that are products between the ladder operators.

For calculating terms on the form $\hat{U}\hat{B}\hat{U}^\dagger$, the Baker-Campbell-Hausdorff (BCH) formula often proves useful. BCH states that for operators $\hat{X}$ and $\hat{Y}$, we have

$$e^{\hat{Y}}\hat{X}e^{-\hat{Y}} = \hat{X} + [\hat{Y},\hat{X}] + \frac{1}{2}[\hat{Y},[\hat{Y},\hat{X}]] + \cdots + \frac{1}{n!}\overbrace{[\hat{Y},[\hat{Y},\ldots[\hat{Y}}^{n},\hat{X}]\ldots]] + \cdots \tag{2.38}$$

There are many unitary transformations that are commonly used to be manipulate Hamiltonians. Two of the most common ones is a unitary transformation to a rotating frame as well as the displacement transformation, which we will now introduce.

2.4.2 Rotating frame transformation

One of the most common unitary transformations is the rotating frame transformation. A rotating frame is often used to move into an interaction picture, but the transformation itself is more general. We illustrate the rotating frame transformation in the case of a single driven qubit, with the Hamiltonian given by (2.11) and the drive Hamiltonian from (2.22):

$$\hat{H} = \omega_q\hat{b}^\dagger\hat{b} - \frac{\alpha}{2}\hat{b}^\dagger\hat{b}^\dagger\hat{b}\hat{b} + \frac{\varepsilon}{2}\left(\hat{b}e^{i\omega_d t} + \hat{b}^\dagger e^{-i\omega_d t}\right), \tag{2.39}$$

The unitary for the rotating frame transformation is

$$\hat{U} = \exp(i\omega_r t\hat{b}^\dagger\hat{b}), \tag{2.40}$$

where ω_r is the frequency of the rotating frame, which gives

$$\frac{\partial \hat{U}}{\partial t} = i\omega_r\hat{b}^\dagger\hat{b}\hat{U}. \tag{2.41}$$

We also need to see how this unitary transforms the annihilation operator $\hat{b}$. The BCH formula motivates us to calculate the commutator

$$[i\omega_r t\hat{b}^\dagger\hat{b},\hat{b}] = i\omega_r t\left(\hat{b}^\dagger\hat{b}\hat{b} - \hat{b}\hat{b}^\dagger\hat{b}\right) = -i\omega_r t\hat{b}, \tag{2.42}$$

where we used the canonical commutation relation $[\hat{b}, \hat{b}^\dagger] = 1$. We see that

$$\overbrace{[i\omega_r t\hat{b}^\dagger\hat{b}, \dots [i\omega_r t\hat{b}^\dagger\hat{b}}^{n}, \hat{b}] \dots] = (-i\omega_r t)^n \hat{b}. \tag{2.43}$$

Inserting this in (2.38) we get

$$\hat{U}\hat{b}\hat{U}^\dagger = \sum_{n=0}^{\infty} \frac{(-i\omega_r t)^n}{n!}\hat{b} = e^{-i\omega_r t}\hat{b}, \tag{2.44}$$

and it follows that $\hat{U}\hat{b}^\dagger\hat{U}^\dagger = \left(\hat{U}\hat{b}\hat{U}^\dagger\right)^\dagger = e^{i\omega_r t}\hat{b}^\dagger$.

Applying (2.36) to our example Hamiltonian (2.39) we arrive at the Hamiltonian in the rotating frame

$$\hat{H} = (\omega_q - \omega_r)\hat{b}^\dagger\hat{b} - \frac{\alpha}{2}\hat{b}^\dagger\hat{b}^\dagger\hat{b}\hat{b} + \frac{\varepsilon}{2}\left(\hat{b}e^{i(\omega_d-\omega_r)t} + \hat{b}^\dagger e^{-i(\omega_d-\omega_r)t}\right). \tag{2.45}$$

We see that the transformation leaves number-conserving terms unaffected, with the exception of the frequency shift of $-\omega_r\hat{b}^\dagger\hat{b}$ from the time-dependence of $\hat{U}$. We can now choose ω_r based on what reference frame we are interested in. A natural choice in this case is to choose $\omega_r = \omega_d$, removing the time dependence from the Hamiltonian. The rotating frame transformation can, as the name suggests, be seen as moving into rotating reference frame in phase space.

For some Hamiltonians, one can not eliminate time-dependence through a rotating frame transformation alone, for example when driving with multiple frequency tones. The rotating wave approximation is an approximation which allows us to neglect time-dependent terms under certain conditions, and is often used in conjunction with the rotating frame transformation.

2.4.3 Rotating wave approximation

The rotating wave approximation (RWA) is an important approximation, first found by Rabi et al. [30] in 1938. At the time the approximation was an experimental finding, without theoretical justification. Since then, many have provided deeper theoretical justification of the RWA through a variety of methods [31].

The RWA states that a term in a Hamiltonian rotating rapidly compared to the resonance frequencies of the system can be ignored. Take for example a model of two interacting cavities

$$\hat{H} = \omega_a\hat{a}^\dagger\hat{a} + \omega_b\hat{b}^\dagger\hat{b} - g(\hat{a} - \hat{a}^\dagger)(\hat{b} - \hat{b}^\dagger). \tag{2.46}$$

Expanding the interaction term and moving into a frame rotating at the cavity frequencies gives

$$\hat{H}_{\text{rf}} = -g\left(e^{-i(\omega_a+\omega_b)t}\hat{a}\hat{b} - e^{-i(\omega_a-\omega_b)t}\hat{a}\hat{b}^\dagger - e^{i(\omega_a-\omega_b)t}\hat{a}^\dagger\hat{b} + e^{i(\omega_a+\omega_b)t}\hat{a}^\dagger\hat{b}^\dagger\right). \tag{2.47}$$

We can see that the $\hat{a}\hat{b}$- and $\hat{a}^\dagger\hat{b}^\dagger$-terms have rotating coefficients with frequency $\omega_a + \omega_b \gg \omega_a, \omega_b$. As long as the timescale of our studied process is long enough, and $g \ll \omega_a, \omega_b$, we can safely ignore these terms as they do not majorly contribute

to the long-term dynamics of the system [20, 31, 32]. In this example this gives the RWA Hamiltonian

$$\hat{H}_{\text{RWA}} = ge^{-i(\omega_a-\omega_b)t}\hat{a}\hat{b}^\dagger + h.c. \tag{2.48}$$

The rotating wave approximation is not perfect, it only holds for weak coupling strengths g, and the accuracy of the approximation is dependent on the state of the system. For example, high photon numbers reduce the accuracy of the approximation [31, 33]. In the presence of drives, the drives have to be near-resonant for the approximation to hold.

2.4.4 Displacement transformation

A displacement transformation can be used to eliminate undesired linear terms in the Hamiltonian. The unitary for a displacement transformation is the displacement operator

$$\hat{\mathcal{D}}(\xi) = \exp[\xi\hat{b}^\dagger - \xi^*\hat{b}], \tag{2.49}$$

where ξ is the amount of displacement. If ξ is time-dependent we have to account for the time-derivative of $\hat{\mathcal{D}}(\xi(t))$ which is

$$\frac{\partial\hat{\mathcal{D}}(\xi(t))}{\partial t} = \left(\dot{\xi}\hat{b}^\dagger - \dot{\xi}^*\hat{b}\right)\hat{\mathcal{D}}(\xi(t)). \tag{2.50}$$

The displacement transformation transforms the annihilation and creation operators as

$$\hat{\mathcal{D}}(\xi)\hat{b}\hat{\mathcal{D}}^\dagger(\xi) = \hat{b} - \xi, \tag{2.51}$$

$$\hat{\mathcal{D}}(\xi)\hat{b}^\dagger\hat{\mathcal{D}}^\dagger(\xi) = \hat{b}^\dagger - \xi^*, \tag{2.52}$$

which can be shown using (2.38). In phase space, the displacement transformation represents a moving reference frame, where the reference frame continuously moves with a velocity determined by α relative to the origin before the transformation.

We highlight how the displacement transformation can be used to cancel linear terms through a simple example. We look at a cavity driven with a sinusoidal microwave drive, described by the Hamiltonian

$$\hat{H} = \omega_a\hat{a}^\dagger\hat{a} + \frac{\varepsilon}{2}\left(\hat{a}e^{i\omega_d t} + \hat{a}^\dagger e^{-i\omega_d t}\right). \tag{2.53}$$

This is a coherent drive applied to a harmonic oscillator, and as such will drive the creation of a coherent state. We can move into a displaced frame with time-dependent displacement $\hat{\mathcal{D}}(\xi(t))$. This gives the transformed Hamiltonian (using (2.36))

$$\hat{H} = \omega_a\hat{a}^\dagger\hat{a} + \left[\left(\frac{\varepsilon}{2}e^{-i\omega_d t} + i\dot{\xi}(t) - \omega_a\xi(t)\right)\hat{a}^\dagger + h.c.\right]. \tag{2.54}$$

We can then eliminate the linear terms by choosing $\xi(t)$ such that it solves the linear ordinary differential equation in the parenthesis in (2.54).

We are now fully equipped to derive an effective Hamiltonian for the SNAPPA gate in Chapter 3.

3
Hamiltonian derivation

In this chapter we aim to derive an effective Hamiltonian for the SNAPPA gate for efficient simulation and analysis of the gate operation. We start from the Hamiltonian for a cavity coupled to a qubit, (2.17), and add the drive Hamiltonian (2.25) for driving the cavity and qubit simulatenously, giving us the initial Hamiltonian

$$\begin{aligned}\hat{H} = \omega_a \hat{a}^\dagger \hat{a} + \omega_q \hat{b}^\dagger \hat{b} - \frac{E_J}{4!}\left[\varphi_q(\hat{b}+\hat{b}^\dagger)\right]^4 - g(\hat{b}-\hat{b}^\dagger)(\hat{a}-\hat{a}^\dagger) \\ + \frac{\varepsilon_1}{2}\left(\hat{b}e^{i\omega_1 t} + \hat{b}^\dagger e^{-i\omega_1 t}\right) + \frac{\varepsilon_2}{2}\left(\hat{a}e^{i\omega_2 t} + \hat{a}^\dagger e^{-i\omega_2 t}\right).\end{aligned} \tag{3.1}$$

We assume to be in the dispersive regime between qubit and cavity, $g/|\omega_q - \omega_a| \ll 1$, which as we noted in Section 2.1.2 means we can write the Hamiltonian as

$$\hat{H} = \omega_a \hat{a}^\dagger \hat{a} + \omega_q \hat{b}^\dagger \hat{b} - \frac{E_J}{4!}\phi^4 + \frac{\varepsilon_1}{2}\left(\hat{b}e^{i\omega_1 t} + \hat{b}^\dagger e^{-i\omega_1 t}\right) + \frac{\varepsilon_2}{2}\left(\hat{a}e^{i\omega_2 t} + \hat{a}^\dagger e^{-i\omega_2 t}\right), \tag{3.2}$$

where

$$\phi = \varphi_q(\hat{b}+\hat{b}^\dagger) + \varphi_a(\hat{a}+\hat{a}^\dagger). \tag{3.3}$$

The frequency of our drives are chosen such that

$$\omega_1 = \omega_q - \Delta, \tag{3.4}$$
$$\omega_2 = \omega_a + \Delta - (n_i+1)\chi. \tag{3.5}$$

in order to drive the $|n_i g\rangle \to |(n_i+1)e\rangle$ transition. The first step of our derivation is to move into a rotating frame.

3.1 Rotating frame transformation

We transform (3.2) into a frame rotating at frequencies ω_1 and ω_2 for qubit and cavity respectively, described by the time-dependent unitary

$$\hat{U}_{\text{rf}} = \exp\left[i\omega_1 t \hat{b}^\dagger \hat{b} + i\omega_2 t \hat{a}^\dagger \hat{a}\right], \tag{3.6}$$

which has the time derivative

$$\frac{\partial \hat{U}_{\text{rf}}}{\partial t} = i(\omega_1 \hat{b}^\dagger \hat{b} + \omega_2 \hat{a}^\dagger \hat{a})\hat{U}_{\text{rf}}. \tag{3.7}$$

As shown for (2.44), this unitary transforms the creation and annihilation operators as

$$\hat{U}_{\text{rf}}\hat{b}\hat{U}_{\text{rf}}^{\dagger} = \hat{b}e^{-i\omega_1 t}, \tag{3.8}$$
$$\hat{U}_{\text{rf}}\hat{b}^{\dagger}\hat{U}_{\text{rf}}^{\dagger} = \hat{b}^{\dagger}e^{i\omega_1 t}, \tag{3.9}$$
$$\hat{U}_{\text{rf}}\hat{a}\hat{U}_{\text{rf}}^{\dagger} = \hat{a}e^{-i\omega_2 t}, \tag{3.10}$$
$$\hat{U}_{\text{rf}}\hat{a}^{\dagger}\hat{U}_{\text{rf}}^{\dagger} = \hat{a}^{\dagger}e^{i\omega_2 t}. \tag{3.11}$$

Transforming the Hamiltonian using $\hat{U}_{\text{rf}}$ according to (2.36) therefore gives

$$\hat{H}_{\text{rf}} = \Delta_1\hat{b}^{\dagger}\hat{b} + \Delta_2\hat{a}^{\dagger}\hat{a} - \frac{E_J}{4!}\tilde{\phi}^4 + \frac{\varepsilon_1}{2}\left(\hat{b} + \hat{b}^{\dagger}\right) + \frac{\varepsilon_2}{2}\left(\hat{a} + \hat{a}^{\dagger}\right), \tag{3.12}$$

where $\tilde{\phi}$ is given by

$$\tilde{\phi} = \hat{U}\phi\hat{U}^{\dagger} = \varphi_q(\hat{b}e^{-i\omega_1 t} + \hat{b}^{\dagger}e^{i\omega_1 t}) + \varphi_a(\hat{a}e^{-i\omega_2 t} + \hat{a}^{\dagger}e^{i\omega_2 t}), \tag{3.13}$$

where φ_q and φ_a are the participation ratios of the qubit and cavity, and Δ_1 and Δ_2 are

$$\Delta_1 = \omega_q - \omega_1 = \Delta, \tag{3.14}$$
$$\Delta_2 = \omega_a - \omega_2 = (n_i + 1)\chi - \Delta. \tag{3.15}$$

Expanding the fourth-order term $\tilde{\phi}^4$ gives many terms in our Hamiltonian, but any term that is not number conserving will have a rapidly rotating time dependence from the rotating frame. They can therefore be ignored according to the rotating wave approximation (Section 2.4.3). The only terms we keep from the expansion is therefore the number conserving terms. We can furthermore define

$$\alpha = \frac{E_J\varphi_q^4}{2}, \tag{3.16}$$
$$K_c = \frac{E_J\varphi_a^4}{2}, \tag{3.17}$$
$$\chi = E_J\varphi_a^2\varphi_q^2, \tag{3.18}$$

which gives us the Hamiltonian in the rotating frame, after the rotating wave approximation:

$$\hat{H}_{\text{rf}} = \Delta_1\hat{b}^{\dagger}\hat{b} + \Delta_2\hat{a}^{\dagger}\hat{a} - \frac{\alpha}{2}\hat{b}^{\dagger}\hat{b}^{\dagger}\hat{b}\hat{b} - \frac{K_c}{2}\hat{a}^{\dagger}\hat{a}^{\dagger}\hat{a}\hat{a} - \chi\hat{b}^{\dagger}\hat{b}\hat{a}^{\dagger}\hat{a} + \frac{\varepsilon_1}{2}\left(\hat{b} + \hat{b}^{\dagger}\right) + \frac{\varepsilon_2}{2}\left(\hat{a} + \hat{a}^{\dagger}\right). \tag{3.19}$$

3.2 Displacement transformation

We now move into a displaced frame. The unitary for a displacement transformation is the displacement operator, (2.49). We displace both qubit and cavity with displacements $\hat{D}_q(\xi_1)$ and $\hat{D}_a(\xi_2)$. The total unitary is therefore

$$\hat{U}_d = \hat{D}_q(\xi_1)\hat{D}_a(\xi_2) = \exp\left[\xi_1\hat{b}^{\dagger} - \xi_1^*\hat{b} + \xi_2\hat{a}^{\dagger} - \xi_2^*\hat{a}\right]. \tag{3.20}$$

This transforms the annihilation and creation operators to

$$\hat{U}_d \hat{a} \hat{U}_d^\dagger = \hat{a} - \xi_1, \tag{3.21}$$
$$\hat{U}_d \hat{a}^\dagger \hat{U}_d^\dagger = \hat{a}^\dagger - \xi_1^*, \tag{3.22}$$
$$\hat{U}_d \hat{b} \hat{U}_d^\dagger = \hat{b} - \xi_2, \tag{3.23}$$
$$\hat{U}_d \hat{b}^\dagger \hat{U}_d^\dagger = \hat{b}^\dagger - \xi_2^*. \tag{3.24}$$

Transforming (3.19) according to (2.36) we get

$$\begin{aligned}\hat{H}' = \Delta_1 \hat{b}^\dagger \hat{b} + \Delta_2 \hat{a}^\dagger \hat{a} - \frac{\alpha}{2} \hat{U}_d \hat{b}^{\dagger 2} \hat{b}^2 \hat{U}_d^\dagger - \frac{K_c}{2} \hat{U}_d \hat{a}^{\dagger 2} \hat{a}^2 \hat{U}_d^\dagger - \chi \hat{U}_d \hat{b}^\dagger \hat{b} \hat{a}^\dagger \hat{a} \hat{U}_d^\dagger \\ + \left[\left(\frac{\varepsilon_1}{2} - \Delta_1 \xi_1 \right) \hat{b}^\dagger + \left(\frac{\varepsilon_2}{2} - \Delta_2 \xi_2 \right) \hat{a}^\dagger + h.c. \right]\end{aligned} \tag{3.25}$$

We can now choose ξ_1 and ξ_2 such that the linear terms in (3.25) disappear. This is accomplished by choosing

$$\xi_1 = \frac{\varepsilon_1}{2\Delta_1}, \tag{3.26}$$
$$\xi_2 = \frac{\varepsilon_2}{2\Delta_2}. \tag{3.27}$$

We must further expand the non-linear terms in (3.25), which we do by inserting the transformed creation and annihilation operators and expanding, ignoring any constant terms. This gives

$$\hat{U} \hat{b}^{\dagger 2} \hat{b}^2 \hat{U}^\dagger = \hat{b}^{\dagger 2} \hat{b}^2 + 4|\xi_1|^2 \hat{b}^\dagger \hat{b} + \left(\xi_1^2 \hat{b}^\dagger \hat{b}^\dagger - 2\xi_1 \hat{b}^\dagger \hat{b}^\dagger \hat{b} - 2\xi_1 |\xi_1|^2 \hat{b}^\dagger + h.c. \right), \tag{3.28}$$
$$\hat{U} \hat{a}^{\dagger 2} \hat{a}^2 \hat{U}^\dagger = \hat{a}^{\dagger 2} \hat{a}^2 + 4|\xi_2|^2 \hat{a}^\dagger \hat{a} + \left(\xi_2^2 \hat{a}^\dagger \hat{a}^\dagger - 2\xi_2 \hat{a}^\dagger \hat{a}^\dagger \hat{a} - 2\xi_2 |\xi_2|^2 \hat{a}^\dagger + h.c. \right), \tag{3.29}$$
$$\begin{aligned}\hat{U} \hat{b}^\dagger \hat{b} \hat{a}^\dagger \hat{a} \hat{U}^\dagger = \hat{b}^\dagger \hat{b} \hat{a}^\dagger \hat{a} + |\xi_2|^2 \hat{b}^\dagger \hat{b} + |\xi_1|^2 \hat{a}^\dagger \hat{a} \\ + \left(\xi_1 \xi_2 \hat{b}^\dagger \hat{a}^\dagger + \xi_1^* \xi_2 \hat{b} \hat{a}^\dagger - \xi_2 \hat{b}^\dagger \hat{b} \hat{a}^\dagger - \xi_1 \hat{b}^\dagger \hat{a}^\dagger \hat{a} - \xi_1 |\xi_2|^2 \hat{b}^\dagger - \xi_2 |\xi_1|^2 \hat{a}^\dagger + h.c. \right).\end{aligned} \tag{3.30}$$

Inserting this gives the effective Hamiltonian

$$\begin{aligned}\hat{H}_{\text{eff}} = \left(\Delta - 2\alpha |\xi_1|^2 - \chi |\xi_2|^2 \right) \hat{b}^\dagger \hat{b} + \left(\chi - \Delta - 2K_c |\xi_2|^2 - \chi |\xi_1|^2 \right) \hat{a}^\dagger \hat{a} \\ - \frac{\alpha}{2} \hat{b}^{\dagger 2} \hat{b}^2 - \frac{K_c}{2} \hat{a}^{\dagger 2} \hat{a}^2 - \chi \hat{b}^\dagger \hat{b} \hat{a}^\dagger \hat{a} \\ + \left[-\frac{\alpha}{2} \left(\xi_1^2 \hat{b}^\dagger \hat{b}^\dagger - 2\xi_1 \hat{b}^\dagger \hat{b}^\dagger \hat{b} \right) - \frac{K_c}{2} \left(\xi_2^2 \hat{a}^\dagger \hat{a}^\dagger - 2\xi_2 \hat{a}^\dagger \hat{a}^\dagger \hat{a} \right) \right. \\ - \chi \left(\xi_1 \xi_2 \hat{b}^\dagger \hat{a}^\dagger + \xi_1^* \xi_2 \hat{b} \hat{a}^\dagger - \xi_2 \hat{b}^\dagger \hat{b} \hat{a}^\dagger - \xi_1 \hat{b}^\dagger \hat{a}^\dagger \hat{a} \right) \\ \left. + \left(\alpha \xi_1 |\xi_1|^2 + \chi \xi_1 |\xi_2|^2 \right) \hat{b}^\dagger + \left(K_c \xi_2 |\xi_2|^2 + \chi \xi_2 |\xi_1|^2 \right) \hat{a}^\dagger + h.c. \right].\end{aligned} \tag{3.31}$$

This effective Hamiltonian only applies when we target a single state transition $|n_i g\rangle \to |(n_i + 1)e\rangle$, but it is constant and therefore efficient to simulate. In order to find an effective Hamiltonian for the more general case when we target multiple transitions at once, we need to account for a more complicated cavity drive.

4
Simulation

In this chapter we aim to simulate (3.31) to verify that it agrees with the experimental data from Kudra et al. [18]. Since (3.31) only holds for a single target Fock state, we can only recreate the data where a single two-photon addition is driven. The available data where this applies consists of amplitude sweeps performed for a single Fock state transition, as well as Stark shift measurements when only a qubit or cavity drive is applied. We also show how the system populations change during the SNAPPA gate, to verify that we are driving the expected two-photon transitions.

Simulating (3.31) implies solving the Schrödinger equation (2.1) numerically for some initial state $|\psi_0\rangle$ with Hamiltonian $\hat{H}_{\text{eff}}$. As mentioned, a quantum state is an element of a Hilbert space $\mathcal{H}$. As long as $\mathcal{H}$ is finite-dimensional we can, in theory, represent states $|\psi\rangle$ as column vectors in $\mathbb{C}^d$ where $d = \dim \mathcal{H}$ and operators as matrices in $\mathbb{C}^{n\times n}$. We can then integrate the Schrödinger equation using ODE integration methods to obtain $|\psi(t)\rangle$ at some time t. However, our Hilbert space is infinite-dimensional due to the infinitely many energy levels in the cavity. Assuming our initial state has a low photon number, we can however truncate the Hilbert space for us to be able to simulate it, under the assumption that higher level energy states are not populated during the operation of the SNAPPA gate. We truncate our Hilbert such that we have 5 energy levels in the qubit and 16 in the cavity, leading to a total Hilbert space dimension of $\dim \mathcal{H} = 5 \times 16 = 80$.

We utilize the Quantum Toolbox in Python [34] (QuTiP) software for simulation. The parameters for our system are taken from Table S1 in [18] and are given in Table 4.1. We note that the drive strengths ε_i are often given in arbitrary units, a.u. The conversion factors from a.u. to physical units is described by β_i, such that $\varepsilon_i = \beta_i \epsilon_i$ where ϵ_i is the drive strengths in arbitrary units. These conversion factors are also shown in Table 4.1.

Parameter	Symbol	Value
Qubit frequency	$\omega_q/2\pi$	5.523 GHz
Cavity frequency	$\omega_a/2\pi$	3.581 GHz
Dispersive shift	$\chi/2\pi$	1.44 MHz
Cavity Kerr	$K_c/2\pi$	2.2 kHz
Qubit anharmonicity	$\alpha/2\pi$	231 MHz
Qubit drive conversion factor	$\beta_q/2\pi$	98.4145 MHz/a.u.
Cavity drive conversion factor	$\beta_a/2\pi$	45.0831 MHz/a.u.

Table 4.1: System parameters for our studied system, taken from Table S1 in Kudra et al. [18].

4.1 Calculation of Stark shifts

When a qubit or cavity is driven by an off-resonant drive, population transfer between the drive and system is minimal. Instead, the drive shifts the resonance frequency of the qubit or cavity. This is known as a Stark shift. Numerically, we can calculate the Stark shift by diagonalizing the Hamiltonian (3.31) when a drive is applied, since the eigenvalues of the Hamiltonian are the energies for the different energy levels. The resonance frequency between the $|0g\rangle$ and $|0e\rangle$ states can then be calculated by taking the difference between their eigenenergies. The Stark shift can then be calculated by comparing this resonance frequency to the resonance frequency in the absence of drives.

This allows us to compare to the Stark shifts from Kudra et al. [18], where the Stark shift of the qubit is measured when only the qubit is driven as well as when only the cavity is driven. We first sweep the qubit drive amplitude ϵ_1 from 0 a.u. to 0.08 a.u., without cavity drive ($\varepsilon_2 = 0$), and calculate the Stark shifts at each step. We use the drive detuning $\Delta = 20$ MHz. We then repeat this process, sweeping ϵ_2 from 0 a.u. to 1 a.u. with no qubit drive. This produces the Stark shifts shown in Figure 4.1.

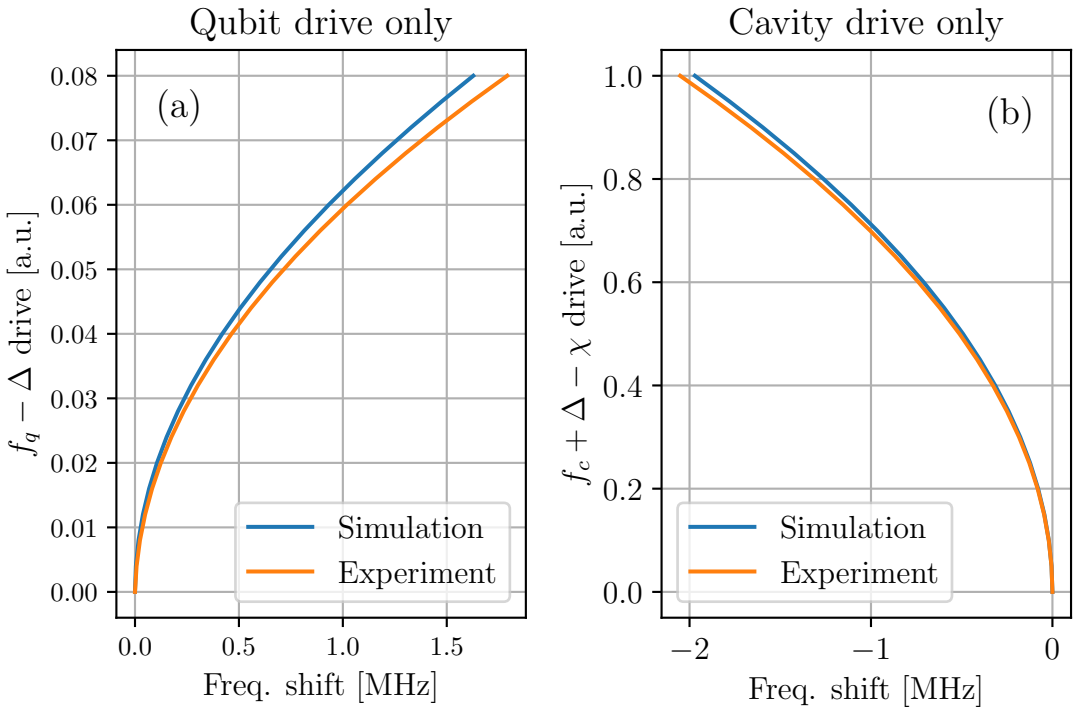

Figure 4.1: Stark shifts from experimental data as well as simulation of (3.31). We calculate the shift when driving with (a) only the qubit drive and (b) only the cavity drive, both with $\Delta = 20$ MHz and system parameters from Table 4.1.

4.2 Simulation of drive amplitude sweeping

From Kudra et al. [18] we have data from sweeping the drive amplitudes for the SNAPPA gate while targeting a single cavity state $|n_i g\rangle$. At each amplitude point we measure the qubit population after a total gate time of $\tau = 4.2$ μs. We then plot this in amplitude space to achieve a chevron pattern for the qubit population at different drive amplitudes $\varepsilon_1, \varepsilon_2$. The amplitude area we sweep is $\epsilon_1 \in [0, 0.08]$ and $\epsilon_2 \in [0, 1]$, both in arbitrary units. Here, the qubit population refers to the probability of measuring the qubit in the $|1\rangle$ state, and is calculated by tracing out the cavity from our state after applying the SNAPPA gate, and then calculating

$$|\langle 1|\psi_q\rangle|^2, \tag{4.1}$$

where $|\psi_q\rangle$ is the state of our qubit after tracing out the cavity.

The chevron patterns available to us from experimental data are from targeting the $|0g\rangle$, $|1g\rangle$, $|2g\rangle$, $|3g\rangle$ and $|5g\rangle$ states respectively. For each of these chevron patterns the cavity frequency is set accordingly, as given by (2.29). For the $|0g\rangle$ and $|2g\rangle$ chevron patterns, we use a drive detuning of $\Delta = 20$ MHz, while for the others we use a drive detuning of $\Delta = 30$ MHz. The results of simulating the amplitude sweeps are shown in Figures 4.2-4.6.

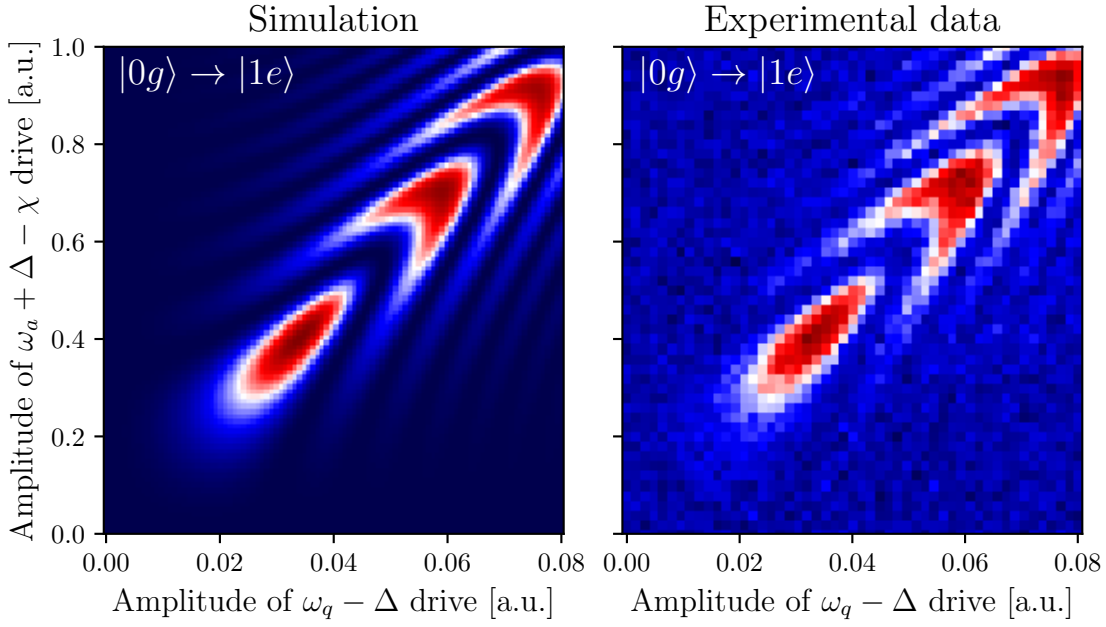

Figure 4.2: Qubit population when sweeping the drive amplitudes for the SNAPPA gate, while targeting the $|0g\rangle \rightarrow |1e\rangle$ two-photon addition, with a drive detuning of $\Delta = 20$ MHz. To the left is data from simulating (3.31), to the right is corresponding experimental data from Kudra et al. [18].

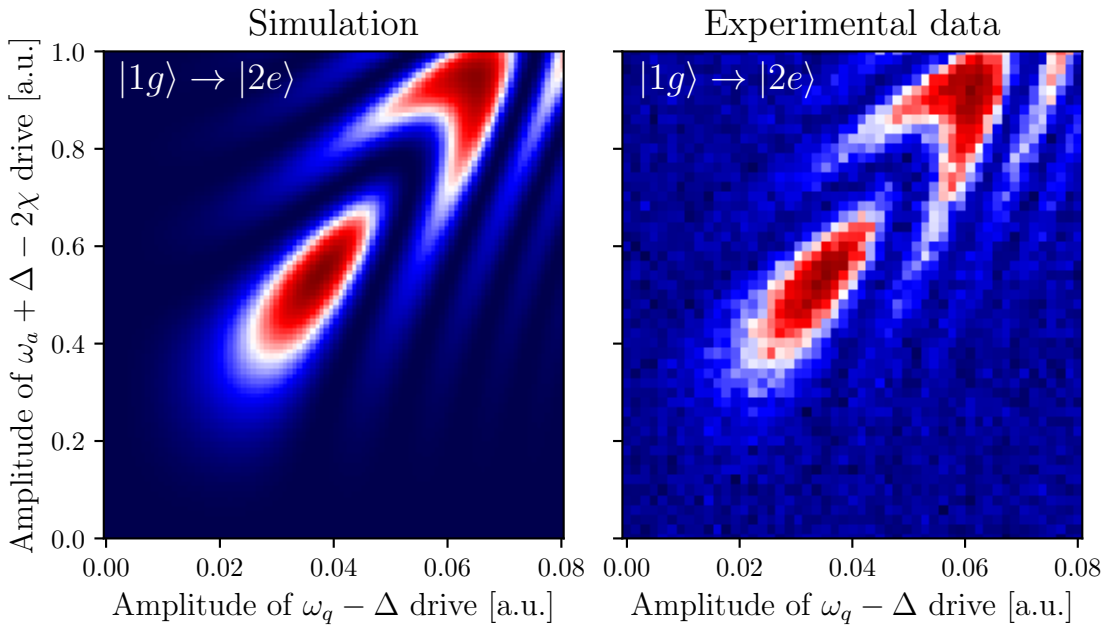

Figure 4.3: Qubit population when sweeping the drive amplitudes for the SNAPPA gate, while targeting the $|1g\rangle \rightarrow |2e\rangle$ two-photon addition, with a drive detuning of $\Delta = 30$ MHz. To the left is data from simulating (3.31), to the right is corresponding experimental data from Kudra et al. [18].

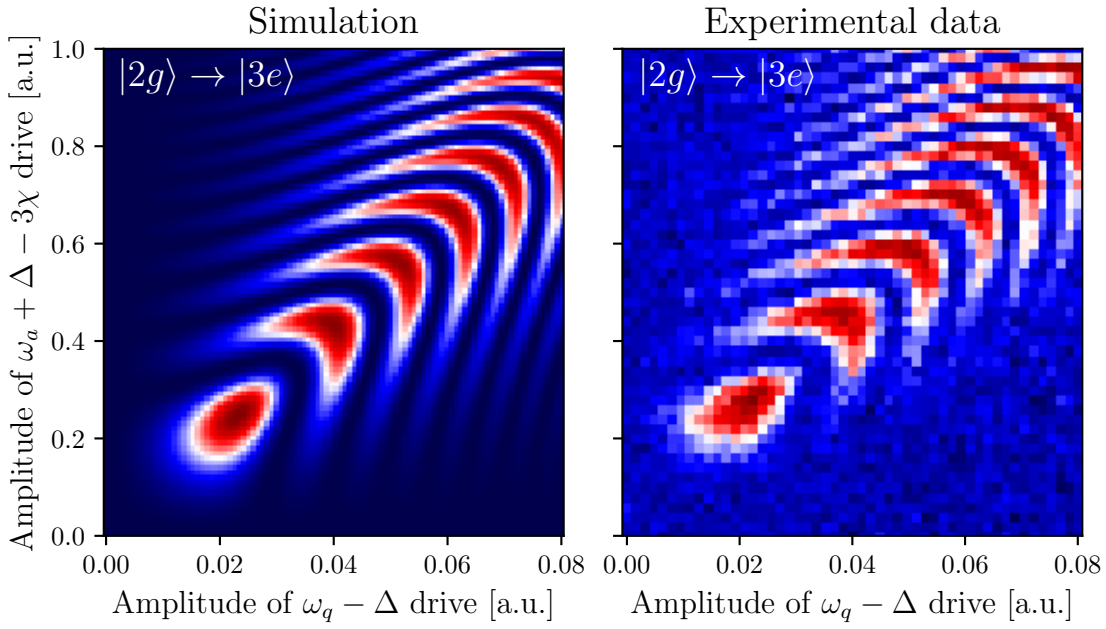

Figure 4.4: Qubit population when sweeping the drive amplitudes for the SNAPPA gate, while targeting the $|2g\rangle \rightarrow |3e\rangle$ two-photon addition, with a drive detuning of $\Delta = 20$ MHz. To the left is data from simulating (3.31), to the right is corresponding experimental data from Kudra et al. [18].

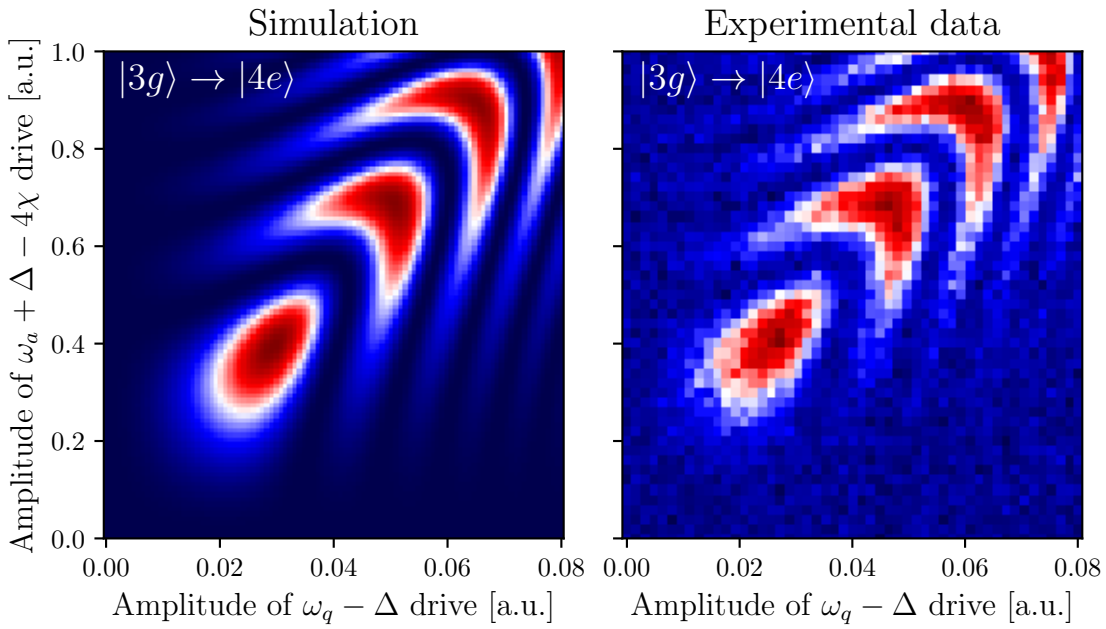

Figure 4.5: Qubit population when sweeping the drive amplitudes for the SNAPPA gate, while targeting the $|3g\rangle \rightarrow |4e\rangle$ two-photon addition, with a drive detuning of $\Delta = 30$ MHz. To the left is data from simulating (3.31), to the right is corresponding experimental data from Kudra et al. [18].

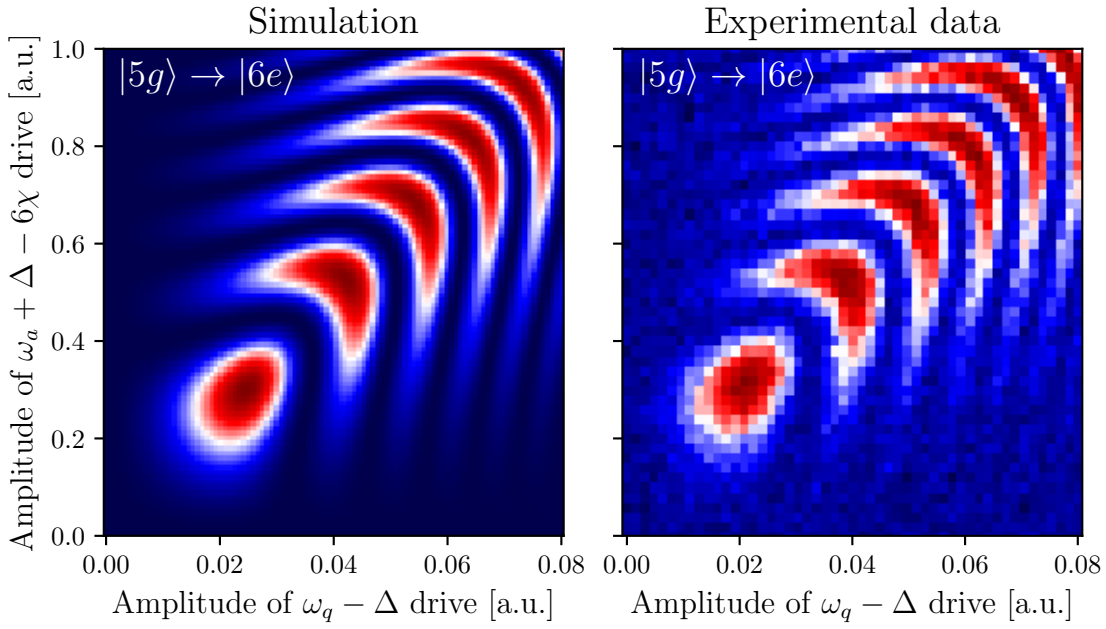

Figure 4.6: Qubit population when sweeping the drive amplitudes for the SNAPPA gate, while targeting the $|5g\rangle \rightarrow |6e\rangle$ two-photon addition, with a drive detuning of $\Delta = 30$ MHz. To the left is data from simulating (3.31), to the right is corresponding experimental data from Kudra et al. [18].

4.3 Population transfer during the SNAPPA gate

In the comparisons to experimental data, we only measure the qubit population. To verify that the system actually undergoes the two-photon transition we expect from the SNAPPA gate we can also plot how the state populations change in the system during the application of the SNAPPA gate. Population here refers to the probability of measuring the system in a specific basis state. As an example, the population of the state $|n_i g\rangle$ is given by

$$|\langle n_i g|\psi\rangle|^2, \tag{4.2}$$

where $|\psi\rangle$ is the state of our system.

This is not possible to measure easily in an experimental setup, but with an accurate model we can accomplish this by keeping track of our system state during the time-evolution of our effective Hamiltonian (3.31), and for each system state calculating (4.2) for each basis state we are interested in.

We do this for all of the transitions simulated in Section 4.2, by choosing the drive amplitudes that maximize the qubit population in the simulated chevron patterns in Figures 4.2-4.6. The resulting population transfers are shown in Figures 4.7-4.11.

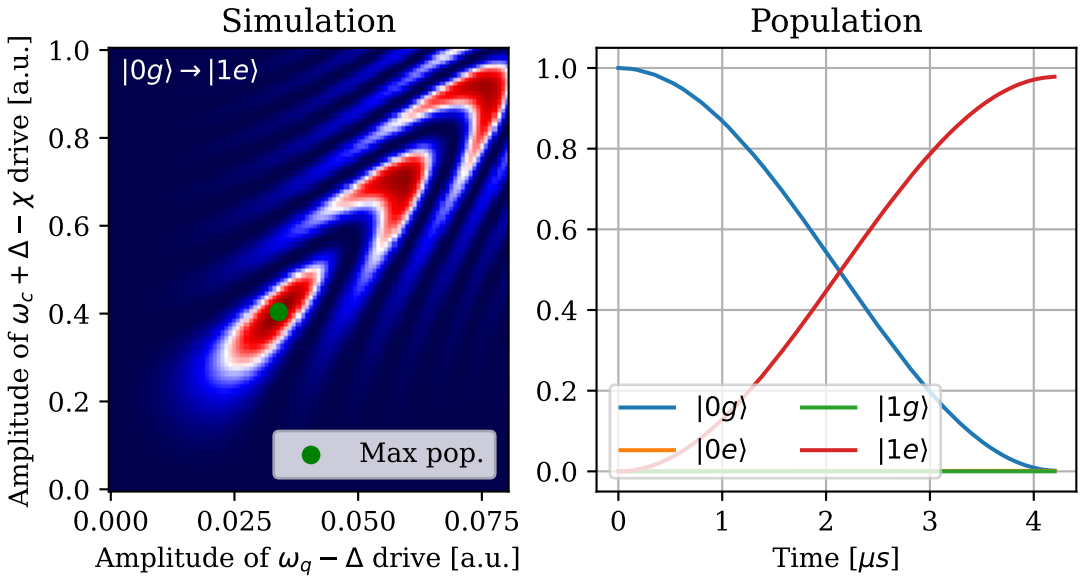

Figure 4.7: Population transfer during the SNAPPA gate while driving the $|0g\rangle \rightarrow |1e\rangle$ transition. The drive amplitudes are taken from the maximal qubit population in Figure 4.2.

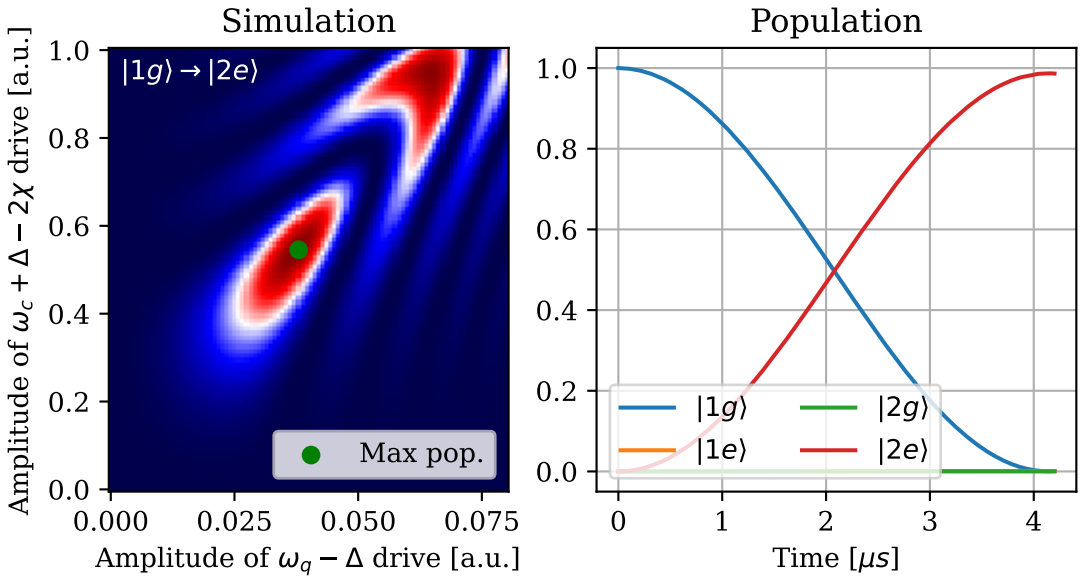

Figure 4.8: Population transfer during the SNAPPA gate while driving the $|1g\rangle \rightarrow |2e\rangle$ transition. The drive amplitudes are taken from the maximal qubit population in Figure 4.3.

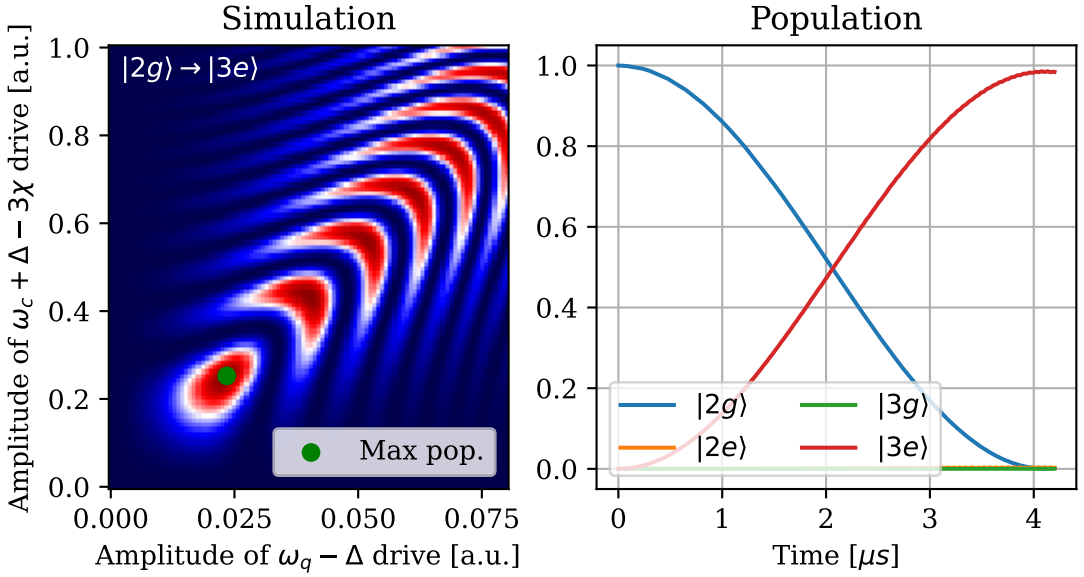

Figure 4.9: Population transfer during the SNAPPA gate while driving the $|2g\rangle \rightarrow |3e\rangle$ transition. The drive amplitudes are taken from the maximal qubit population in Figure 4.4.

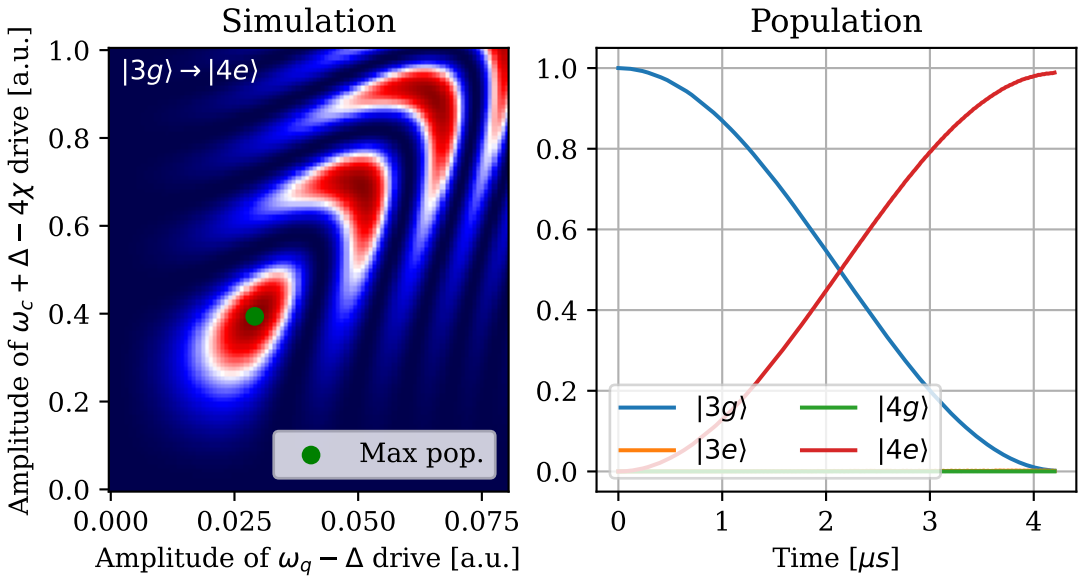

Figure 4.10: Population transfer during the SNAPPA gate while driving the $|3g\rangle \rightarrow |4e\rangle$ transition. The drive amplitudes are taken from the maximal qubit population in Figure 4.5.

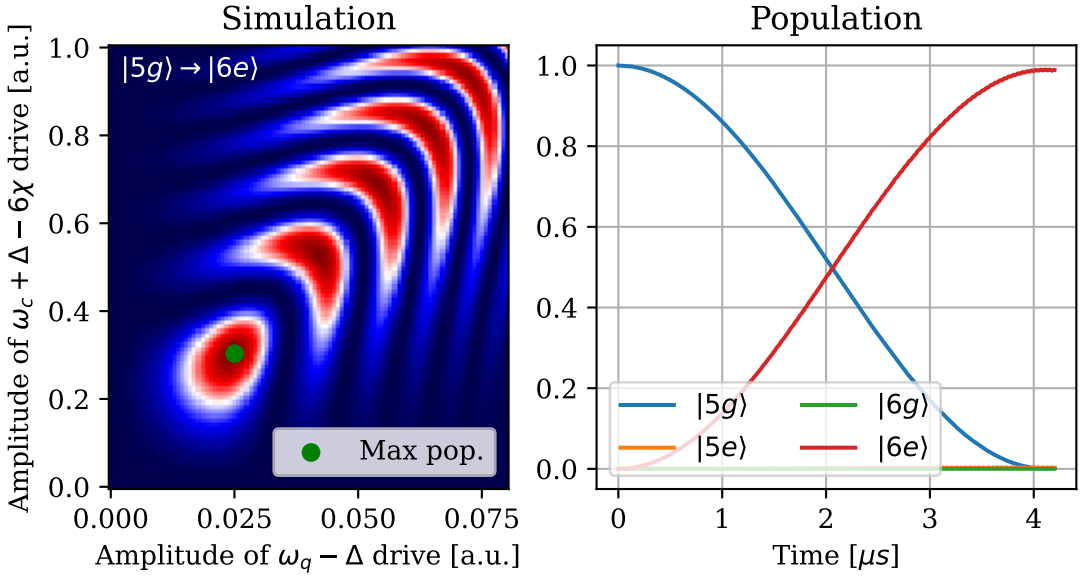

Figure 4.11: Population transfer during the SNAPPA gate while driving the $|5g\rangle \rightarrow |6e\rangle$ transition. The drive amplitudes are taken from the maximal qubit population in Figure 4.6.

5

Discussion

We have presented a new effective Hamiltonian, (3.31), for the SNAPPA gate. We can see from our simulations in Chapter 4 that our derived Hamiltonian matches closely with experimental data, without any fitting parameters or additional terms. From Section 4.3 we can also see that the effective Hamiltonian does indeed drive the two-photon transition we expect from the SNAPPA gate. In this chapter we discuss our results, as well as the qualitative difference between our derivation and the erroneous one in Kudra et al. [18].

5.1 Analyzing the effective Hamiltonian

The SNAPPA gate aims to drive a two-photon addition to the qubit and cavity. This process can be described using the action of $\hat{b}^\dagger\hat{a}^\dagger$, which as we can see in (3.31) has an effective drive strength of $g_{\text{eff}} = \chi\xi_1\xi_2$, where

$$\xi_1 = \frac{\varepsilon_1}{2\Delta_1},$$
$$\xi_2 = \frac{\varepsilon_2}{2\Delta_2}.$$

The strength of this desired interaction is therefore proportional to both drive strengths and the dispersive shift χ.

All of the off-diagonal terms, including our desired interaction, stem from the non-linearities of the system. The non-linearities cause different Fock states in the cavity to dephase from one another. It is reasonable to suspect that the off-diagonal terms in (3.31) is this dephasing effect in the displaced frame. The effective Hamiltonian (3.31) is therefore not only useful for the SNAPPA gate, but is a general model for a cavity coupled to a transmon, with single-tone off-resonant drives applied to each.

The other off-diagonal elements in (3.31), with the exception of $\hat{b}^\dagger\hat{a}^\dagger$, drive undesireable transitions in the system, and can therefore be regarded as error terms in the context of the SNAPPA gate. We note that there are primarily three different types of error terms present in (3.31). The first are two-photon transitions in only the qubit or cavity, driven by the $\hat{b}^\dagger\hat{b}^\dagger$- and $\hat{a}^\dagger\hat{a}^\dagger$-terms. These are proportional to ξ_1^2 and ξ_2^2 respectively, as well as their corresponding anharmonic coefficients α and K_c.

Due to the quadratic dependence of drive strength, these error terms suggest that it is undesirable to drive the system harder than necessary; one should use the

lowest drive amplitudes possible to drive the SNAPPA gate in order to minimize these error terms. This also might explain why the qubit drive amplitude is much smaller than the cavity drive amplitude. We can obtain a certain effective drive strength g_{eff} by varying ξ_1 and ξ_2 in proportion to each other. Since $\alpha \gg K_c$, it is beneficial to choose a larger cavity drive strength than qubit drive strength to obtain the same g_{eff}, as this minimizes the effective strength of the two-photon error terms.

The second type of error term is a photon exchange between qubit and cavity, mediated by the drives. It is described by the action of $\hat{b}\hat{a}^\dagger + h.c.$, with an effective drive strength of $\chi\xi_1^*\xi_2 = \chi\xi_1\xi_2 = g_{\text{eff}}$, since ξ_1 is real. This term could potentially be compensated for by a good choice of gate time τ in combination with drive strengths, but so far this has not been investigated.

Finally, the third type of error term are single-photon transitions, described by the remaining non-diagonal terms in (3.31). There are many of these terms, including number dependent single-photon transition terms, e.g. the $\hat{b}^\dagger\hat{b}^\dagger\hat{b}$- and $\hat{b}^\dagger\hat{a}^\dagger\hat{a}$-terms, which are single-photon transitions that are number dependent on the qubit and cavity photon number respectively. Due to the many different terms it is difficult to accurately predict their contribution to the process, but since many of these terms have rather strong drive strengths, such as $\alpha\xi_1|\xi_1|^2$, it is reasonable to suspect that single-photon transitions might be the dominant source of error in (3.31).

5.2 Comparison with previous Hamiltonian

In Kudra et al. [18] they present the effective Hamiltonian (2.30). Without the fitting parameters and moving to a frame rotating at the drive frequencies rather than the resonance frequencies, (2.30) becomes

$$\begin{aligned}\hat{H}(t) = &\left(\Delta_1 - 2\alpha|\xi_1|^2 - \chi|\xi_2|^2\right)\hat{b}^\dagger\hat{b} + \left(\Delta_2 - 2K_c|\xi_2|^2 - \chi|\xi_1|^2\right)\hat{a}^\dagger\hat{a} \\ &-\frac{\alpha}{2}\hat{b}^{\dagger 2}\hat{b}^2 - \frac{K_c}{2}\hat{a}^{\dagger 2}\hat{a} - \chi\hat{b}^\dagger\hat{b}\hat{a}^\dagger\hat{a} + \left[-\chi\xi_1\xi_2\hat{b}^\dagger\hat{a}^\dagger + h.c.\right],\end{aligned} \tag{5.1}$$

where

$$\xi_1 = \frac{\varepsilon_1}{2\Delta_1},\ \xi_2 = \frac{\varepsilon_2}{2\Delta_2}. \tag{5.2}$$

We note that (5.1) has the same coefficient for the $\hat{b}^\dagger\hat{a}^\dagger$-term as (3.31), yet lacks many of the other terms. Simulating (5.1) without any fitting parameters for the $|0g\rangle \to |1e\rangle$ transition yields Figure 5.1 which does not agree with the experimental data from Figure 4.2.

It is interesting to discuss why the derivation of (5.1) fails, as the method used is often utilized in the analysis of qubit-cavity systems and has failed to agree with experimental results before, for example in reference [19]. The approach to deriving (5.1) is very similar to the approach used in Chapter 3, the only difference being the order of transformations. In Kudra et al. [18] (Appendix S3) they approach the derivation by first performing a time-dependent displacement transformation, followed by the rotating wave approximation and only then moving into a rotating

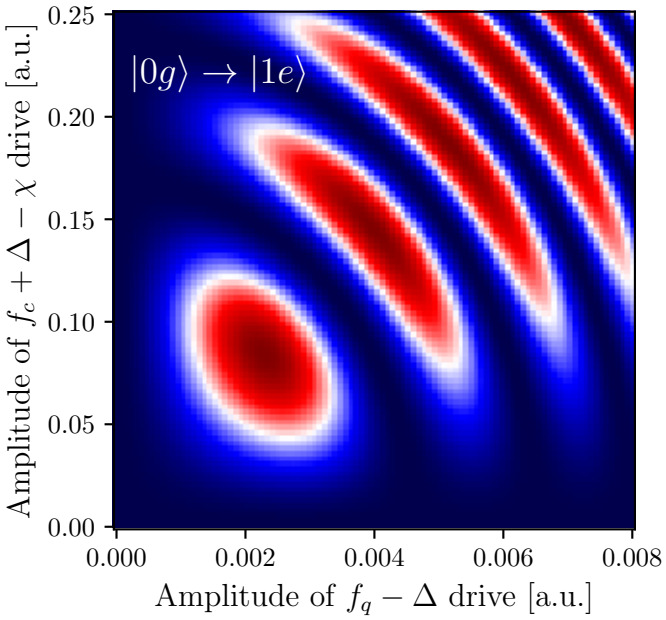

Figure 5.1: Qubit population from amplitude sweep for the $|0g\rangle \rightarrow |1g\rangle$ two-photon addition. Simulated using the effective Hamiltonian derived in Kudra et al. [18], which fails to match the experimental data in Figure 4.2.

frame. The displacement transformation has to be time-dependent in order to eliminate the time-dependent coefficients in the drive Hamiltonian. This displacement is

$$\xi_1 = \frac{\varepsilon_1}{2\Delta_1} e^{-i\omega_1 t}, \tag{5.3}$$

$$\xi_2 = \frac{\varepsilon_2}{2\Delta_2} e^{-i\omega_2 t}. \tag{5.4}$$

After the displacement transformation they get many time-dependent terms from the transformation of the non-linear terms $\hat{b}^\dagger\hat{b}^\dagger\hat{b}\hat{b}$, $\hat{a}^\dagger\hat{a}^\dagger\hat{a}\hat{a}$ and $\hat{b}^\dagger\hat{b}\hat{a}^\dagger\hat{a}$ (see (3.28)-(3.30)), where the time dependence comes from ξ_1 and ξ_2. In Kudra et al. [18] as well as Campagne-Ibarcq et al. [19], they then remove many of these time-dependent terms using the rotating wave approximation as the terms are rapidly rotating. The only terms that are kept are those of interest for the relevant interaction for reasons that will be obvious soon. In the case of SNAPPA this term is

$$\chi\xi_1\xi_2 e^{-i(\omega_1+\omega_2)t}\hat{b}^\dagger\hat{a}^\dagger + h.c. \tag{5.5}$$

Moving into a rotating frame rotating at the drive frequencies then gives us (5.1), as the rotating frame cancels the time-dependence of (5.5), hence why this term was kept.

The error in this derivation is an invalid application of the rotating wave approximation. All of the terms in the expansion of the non-linear terms are in fact resonant with the system, which can be seen when moving into the rotating frame. Just as the rotating coefficient of (5.5) is cancelled by the rotating frame, so are

the corresponding coefficients in the other expanded terms. Accounting for all the terms in the expansion we arrive at the correct effective Hamiltonian (3.31). This suggests that one should be careful when applying the RWA in a displaced frame, as the true resonance conditions of the system are not obvious. It highlights the usefulness of the rotating frame as a tool to see which interactions are resonant and which ones can be neglected by invoking the RWA.

5.3 Conclusion and outlook

In conclusion, we have found an effective Hamiltonian which accurately describes the dynamics of the SNAPPA gate, demonstrated through numerical simulations which closely match the experimental data from Kudra et al. [18]. We have identified that the error in the previous theoretical derivation is a matter of invalid application of the rotating wave approximation at a premature stage in the displaced frame. We believe this to also be of interest for several other derivations in similar quantum systems, such as that described in Campagne-Ibarcq et al. [19].

Using the effective Hamiltonian, we have also identified several sources of error for the SNAPPA gate, which can help to model more effective drive protocols through optimal control methods. This also gives us a good initial model for describing other processes to apply after a SNAPPA gate, such fast qubit reset in order to implement an autonomous quantum error correction scheme for bosonic codes [18].

The derived model is not unique for the SNAPPA gate, it is a general model for a qubit coupled to a microwave cavity in the dispersive regime, being driven by off-resonant classical drives in a single frequency mode. As such, it can be used for modelling and optimal control for not only the SNAPPA gate but other processes and operations. The insights from the derivation might also help with modelling more complicated systems.

The model is a step in the direction of a full model for the SNAPPA gate, where we include the simultaneous targeting of multiple cavity Fock states, which requires more advanced modelling techniques due to the frequency comb drive applied to the cavity. We are hopeful that the model will prove useful for the modelling and simulation of fast qubit reset for the qubit-cavity system, which is the next step towards realizing AQEC using the SNAPPA gate.

Bibliography

[1]R. P. Feynman, "Simulating physics with computers", International Journal of Theoretical Physics **21**, 467–488 (1982).

[2]P. Shor, "Algorithms for quantum computation: discrete logarithms and factoring", in Proceedings 35th Annual Symposium on Foundations of Computer Science (1994), pp. 124–134.

[3]B. P. Lanyon, J. D. Whitfield, G. G. Gillett, M. E. Goggin, M. P. Almeida, I. Kassal, J. D. Biamonte, M. Mohseni, B. J. Powell, M. Barbieri, A. Aspuru-Guzik, and A. G. White, "Towards quantum chemistry on a quantum computer", Nature Chemistry **2**, 106–111 (2010).

[4]H. R. Moser, "The quantum mechanical solution of the traveling salesman problem", Physica E: Low-dimensional Systems and Nanostructures **16**, 280–285 (2003).

[5]P. Krantz, M. Kjaergaard, F. Yan, T. P. Orlando, S. Gustavsson, and W. D. Oliver, "A quantum engineer's guide to superconducting qubits", Applied Physics Reviews **6**, 021318 (2019).

[6]A. Joshi, K. Noh, and Y. Y. Gao, "Quantum information processing with bosonic qubits in circuit QED", Quantum Science and Technology **6**, 033001 (2021).

[7]A. G. Fowler, M. Mariantoni, J. M. Martinis, and A. N. Cleland, "Surface codes: Towards practical large-scale quantum computation", Physical Review A **86**, 032324 (2012).

[8]S. Krastanov, V. V. Albert, C. Shen, C.-L. Zou, R. W. Heeres, B. Vlastakis, R. J. Schoelkopf, and L. Jiang, "Universal control of an oscillator with dispersive coupling to a qubit", Physical Review A **92**, 040303 (2015).

[9]R. W. Heeres, B. Vlastakis, E. Holland, S. Krastanov, V. V. Albert, L. Frunzio, L. Jiang, and R. J. Schoelkopf, "Cavity State Manipulation Using Photon-Number Selective Phase Gates", Physical Review Letters **115**, 137002 (2015).

[10]Z. Leghtas, G. Kirchmair, B. Vlastakis, R. J. Schoelkopf, M. H. Devoret, and M. Mirrahimi, "Hardware-Efficient Autonomous Quantum Memory Protection", Physical Review Letters **111**, 120501 (2013).

[11]M. Mirrahimi, Z. Leghtas, V. V. Albert, S. Touzard, R. J. Schoelkopf, L. Jiang, and M. H. Devoret, "Dynamically protected cat-qubits: a new paradigm for universal quantum computation", New Journal of Physics **16**, 045014 (2014).

[12]M. H. Michael, M. Silveri, R. T. Brierley, V. V. Albert, J. Salmilehto, L. Jiang, and S. M. Girvin, "New Class of Quantum Error-Correcting Codes for a Bosonic Mode", (2016).

[13]N. Ofek, A. Petrenko, R. Heeres, P. Reinhold, Z. Leghtas, B. Vlastakis, Y. Liu, L. Frunzio, S. M. Girvin, L. Jiang, M. Mirrahimi, M. H. Devoret, and R. J. Schoelkopf,

"Extending the lifetime of a quantum bit with error correction in superconducting circuits", Nature **536**, 441–445 (2016).
[14]L. Hu, Y. Ma, W. Cai, X. Mu, Y. Xu, W. Wang, Y. Wu, H. Wang, Y. P. Song, C.-L. Zou, S. M. Girvin, L.-M. Duan, and L. Sun, "Quantum error correction and universal gate set operation on a binomial bosonic logical qubit", Nature Physics **15**, 503–508 (2019).
[15]J. Cohen, W. C. Smith, M. H. Devoret, and M. Mirrahimi, "Degeneracy-Preserving Quantum Nondemolition Measurement of Parity-Type Observables for Cat Qubits", Physical Review Letters **119**, 060503 (2017).
[16]F. Reiter, A. S. Sørensen, P. Zoller, and C. A. Muschik, "Dissipative quantum error correction and application to quantum sensing with trapped ions", Nature Communications **8**, 1822 (2017).
[17]J. M. Gertler, B. Baker, J. Li, S. Shirol, J. Koch, and C. Wang, "Protecting a bosonic qubit with autonomous quantum error correction", Nature **590**, 243–248 (2021).
[18]M. Kudra, T. Abad, M. Kervinen, A. M. Eriksson, F. Quijandría, P. Delsing, and S. Gasparinetti, *Experimental realization of deterministic and selective photon addition in a bosonic mode assisted by an ancillary qubit*, (Dec. 22, 2022) `http://arxiv.org/abs/2212.12079` (visited on 11/21/2023), preprint.
[19]P. Campagne-Ibarcq, E. Zalys-Geller, A. Narla, S. Shankar, P. Reinhold, L. Burkhart, C. Axline, W. Pfaff, L. Frunzio, R. J. Schoelkopf, and M. H. Devoret, "Deterministic Remote Entanglement of Superconducting Circuits through Microwave Two-Photon Transitions", Physical Review Letters **120**, 200501 (2018).
[20]R. Manenti and M. Motta, *Quantum information science* (Oxford University Press, Oxford, 2023), 740 pp.
[21]D. J. Griffiths and D. F. Schroeter, *Introduction to Quantum Mechanics*, 3rd ed. (Cambridge University Press, Aug. 16, 2018).
[22]X. Gu, A. F. Kockum, A. Miranowicz, Y.-x. Liu, and F. Nori, "Microwave photonics with superconducting quantum circuits", Physics Reports **718–719**, 1–102 (2017).
[23]H. Haffner, C. Roos, and R. Blatt, "Quantum computing with trapped ions", Physics Reports **469**, 155–203 (2008).
[24]A. Chatterjee, P. Stevenson, S. De Franceschi, A. Morello, N. P. De Leon, and F. Kuemmeth, "Semiconductor qubits in practice", Nature Reviews Physics **3**, 157–177 (2021).
[25]A. Blais, A. L. Grimsmo, S. M. Girvin, and A. Wallraff, "Circuit Quantum Electrodynamics", Reviews of Modern Physics **93**, 025005 (2021).
[26]M. Malekakhlagh, A. Petrescu, and H. E. Türeci, "Lifetime renormalization of weakly anharmonic superconducting qubits. I. Role of number nonconserving terms", Physical Review B **101**, 134509 (2020).
[27]D. Gottesman, A. Kitaev, and J. Preskill, "Encoding a qubit in an oscillator", Physical Review A **64**, 012310 (2001).
[28]W.-L. Ma, S. Puri, R. J. Schoelkopf, M. H. Devoret, S. Girvin, and L. Jiang, "Quantum control of bosonic modes with superconducting circuits", Science Bulletin **66**, 1789–1805 (2021).

[29]A. M. Eriksson, T. Sépulcre, M. Kervinen, T. Hillmann, M. Kudra, S. Dupouy, Y. Lu, M. Khanahmadi, J. Yang, C. Castillo-Moreno, P. Delsing, and S. Gasparinetti, "Universal control of a bosonic mode via drive-activated native cubic interactions", Nature Communications **15**, 2512 (2024).
[30]I. I. Rabi, J. R. Zacharias, S. Millman, and P. Kusch, "A New Method of Measuring Nuclear Magnetic Moment", Physical Review **53**, 318–318 (1938).
[31]D. Burgarth, P. Facchi, R. Hillier, and M. Ligabò, "Taming the Rotating Wave Approximation", Quantum **8**, 1262 (2024).
[32]U. Haeberlen and J. S. Waugh, "Coherent Averaging Effects in Magnetic Resonance", Physical Review **175**, 453–467 (1968).
[33]D. Walls, "Higher order effects in the single atom field mode interaction", Physics Letters A **42**, 217–218 (1972).
[34]J. Johansson, P. Nation, and F. Nori, "QuTiP 2: A Python framework for the dynamics of open quantum systems", Computer Physics Communications **184**, 1234–1240 (2013).

DEPARTMENT OF SOME SUBJECT OR TECHNOLOGY
CHALMERS UNIVERSITY OF TECHNOLOGY
Gothenburg, Sweden
www.chalmers.se

CHALMERS
UNIVERSITY OF TECHNOLOGY